Bulk microphysical properties of semi-transparent cirrus from AIRS: a six year global climatology and statistical analysis in synergy with geometrical profiling data from CloudSat-CALIPSO

A. Guignard, C. J. Stubenrauch, A. J. Baran, Raymond Armante

Atmos. Chem. Phys., 12, 503–525, 2012
www.atmos-chem-phys.net/12/503/2012/
doi:10.5194/acp-12-503-2012

Atmospheric Chemistry and Physics

Bulk microphysical properties of semi-transparent cirrus from AIRS: a six year global climatology and statistical analysis in synergy with geometrical profiling data from CloudSat-CALIPSO

A. Guignard[1], **C. J. Stubenrauch**[1], **A. J. Baran**[2], **and R. Armante**[1]

[1]Laboratoire de Météorologie Dynamique, Ecole Polytechnique, Palaiseau, France
[2]Met Office, Fitzroy Road, Exeter, EX1 3PB, UK

Correspondence to: A. Guignard (anthony.guignard@lmd.polytechnique.fr)

Received: 30 July 2011 – Published in Atmos. Chem. Phys. Discuss.: 1 September 2011
Revised: 9 December 2011 – Accepted: 21 December 2011 – Published: 10 January 2012

Abstract. This article presents a retrieval method and a statistical analysis of the bulk microphysical properties of semi-transparent ice clouds using the Atmospheric Infrared Sounder (AIRS). The method relies on spectral differences of cirrus emissivities in the 8–12 µm range and is sensitive to the effective ice crystal diameter (D_e) and ice water path (IWP) of up to 85 µm and 120 g m^{-2}, respectively. An indication of the most frequent ice crystal habit in the cirrus has been obtained by using separately single scattering properties of column-like and aggregate-like ice crystals in the simulations. Uncertainties due to hypotheses on atmospheric parameters and ice crystal single scattering properties are discussed and the cirrus emissivity and temperature range for the applicability of the method are determined. To be sure that the cirrus only includes ice crystals, one has to restrict the cloud temperature range to $T_{cld} < 230$ K. On a global scale, these semi-transparent ice clouds (cirrus) represent about 25 % of all high clouds and are mainly encountered in the midlatitudes during winter and in the tropics, with an average D_e and IWP of 52 µm and 27 g m^{-2}, respectively. A comparison with bulk microphysical properties from the TIROS-N Operational Vertical Sounder (TOVS) shows an agreement on global mean values. The addition of spectral information revealed improvements at the limits of the cirrus emissivity range. Collocated Radar-Lidar Geometrical Profiling (GEOPROF) data have been used to study the vertical structure of these clouds and to infer average ice water content (IWC) for cirrus with a small vertical extent. This allowed us to compare and contrast parameterizations of D_e as functions of IWC and IWP, respectively.

1 Introduction

High clouds (with cloud pressure smaller than 440 hPa) cover about 30 % of the globe (e.g. Wylie and Menzel., 1999; Wylie et al., 2005; Stubenrauch et al., 2006, 2010; Chepfer et al., 2010) and therefore strongly influence the radiation budget of the Earth. Depending on the formation process of cirrus clouds (large-scale lifting, convection, atmospheric waves (e.g. Ivanova et al., 2001; Stith et al., 2002; Boehm et al., 2003; Luo and Rossow, 2004), one expects that their resulting microphysical and macrophysical properties should be different. In General Circulation Models (GCM), D_e is often parameterized as a function of IWC or cloud temperature using some deterministic polynomial fit (e.g. McFarlane et al., 1992; Donner et al., 1997; Bony et al., 2001; Edwards et al., 2007). Cloud optical properties are then calculated from the GCM diagnosed D_e, assuming a single ice crystal habit. The former parameterizations are based on only a few field campaigns located about the Earth and for very limited time periods (Heymsfield and Platt, 1984; Korolev et al., 2001; Boudala et al., 2002; McFarquhar et al., 2003; Garrett et al., 2004). Moreover, recent studies by (Korolev and Isaac, 2004; Field et al., 2006; McFarquhar et al., 2007) have demonstrated that the particle size distribution (PSD) data on which the former parameterizations are based are probably biased to smaller D_e values due to the shattering of ice crystals on the probe inlets. Even if satellite observations only allow a retrieval of bulk microphysical properties which relies on various assumptions, they provide a unique possibility to study geographical distributions and seasonal variability of D_e and IWP as well as relationships between D_e, IWP and cloud physical properties and thermodynamic properties of the atmosphere over the whole globe.

Published by Copernicus Publications on behalf of the European Geosciences Union.

Compared to other passive remote sensing instruments, the high spectral resolution infrared (IR) vertical sounders provide reliable properties of cirrus with a visible optical depth as low as 0.1, day and night (Wylie and Menzel, 1994; Ackerman et al., 1995; Stubenrauch et al., 1999; Chung et al., 2000; Kahn et al., 2004, 2007; Stubenrauch et al., 2010). CO_2-sensitive channels of IR vertical sounders allow the determination of cloud height and cloud emissivity, and cloud spectral emissivity differences in the 8–12 µm range allows an estimation of the D_e and IWP of semi-transparent cirrus (e.g. Rädel et al., 2003; Kahn et al., 2008; Pavolonis, 2010). IR sounders have continuously observed our planet since 1979, with improvements in spectral resolution: the TIROS-N Operational Vertical Sounders (Smith et al., 1979) onboard the NOAA polar satellites, the Atmospheric InfraRed Sounder (Chahine et al., 2006) onboard Aqua (since 2002) and the InfraRed Atmospheric Sounding Interferometer (Hilton et al., 2012) onboard METOP (since 2006). Once the cloud physical properties (cloud pressure and emissivity) are retrieved, cirrus bulk microphysical properties D_e and IWP may be determined based on their spectral emissivity difference. Whereas techniques combining visible (VIS) and near IR (NIR) information (e.g. Platnick et al., 2003; Roebeling et al., 2006; Hong et al., 2007) provide estimations of D_e and IWP for all ice clouds, IR techniques, based essentially on spectral absorption differences, are restricted to semi-transparent ice clouds. However, uncertainties due to ice crystal habit are smaller than in the VIS-NIR techniques (e.g. Cooper et al., 2007), and they may be retrieved day and night. In this article we present a retrieval method of cirrus bulk microphysical properties D_e and IWP based on cirrus spectral emissivities. For their determination the retrieved cloud pressure is necessary. This retrieval extends the retrieval of cloud physical properties using AIRS (Stubenrauch et al., 2010). Compared to earlier retrievals using observations from TOVS (Stubenrauch et al., 1999; Rädel et al., 2003), the use of more spectral channels with AIRS allows an indication of the most frequent ice crystal habit in the cirrus (by distinguishing column-like and aggregate-like ice crystals in the simulations). Simultaneous geometrical profiling (GEOPROF) data (Mace et al., 2009) using combined measurements of the active lidar and radar of the missions CALIPSO (Winker et al., 2003) and CloudSat (Stephens et al., 2002) allow us to characterize the cirrus vertical structure and to study relationships with the bulk microphysical properties.

This article is structured in the following way: Data and retrieval methods are described in Sect. 2. After sensitivity studies in Sect. 3, we discuss the retrieval applicability in Sect. 4. Section 5 first presents geographical distributions and seasonal variations of the occurrence of semi-transparent cirrus and their physical and microphysical properties. Secondly, comparisons are presented against TOVS and relationships between D_e and IWP (IWC) are explored. The latter has been estimated from IWP and cloud vertical extent for cirrus with a relatively small vertical extent (less than 2 km). Our findings are summarized in Sect. 6.

2 Data and methods

2.1 AIRS cloud properties

Launched in May 2002 onboard the Earth Observing System (EOS) platform Aqua, the AIRS instrument (Aumann et al., 2003; Chahine et al., 2006) provides very high spectral resolution measurements of Earth-emitted radiation in three spectral bands (3.74–4.61 µm, 6.20–8.22 µm and 8.80–15.40 µm), using 2378 channels with a spectral resolution given by $\Delta\lambda/\lambda = 0.0008$. The polar orbiting Aqua satellite provides observations at 01:30 and 13:30 local time (LT, equator crossing time). The spatial resolution of these measurements is 13.5 km at nadir. Nine AIRS measurements (3×3) correspond to one footprint of the Advanced Microwave Sounder Unit (AMSU). NASA level 2 (L2, version 5) atmospheric temperature and water vapour profiles (Susskind et al., 2003, 2006) are retrieved from cloud-cleared AIRS radiances (Chahine et al., 2006) within each AMSU footprint. We have averaged the atmospheric profiles of good quality (Tobin et al., 2006) on a 1°latitude × 1°longitude grid; and if no data are available, weekly running means are included.

The cloud property retrieval (presented in Fig. 1) developed at the Laboratoire de Météorologie Dynamique (LMD) provides cloud pressure and emissivity of a single cloud layer (of the uppermost cloud layer in the case of multilayer clouds). It is based on a weighted χ^2 (χ^2_w) method using eight AIRS radiances in the range 11–13 µm, sounding along the wing of the 15 µm CO_2 absorption band (Stubenrauch et al., 2010). These calibrated radiances are provided by NASA (level 1B, version 5). The χ^2_w method determines the pressure level p_{cld} for which the measured radiances at all wavelengths provide the most coherent cloud emissivity, ϵ_{cld}:

$$\epsilon_{cld}(p_k, \lambda_i) = \frac{I_m(\lambda_i) - I_{clr}(\lambda_i)}{I_{cld}(p_k, \lambda_i) - I_{clr}(\lambda_i)} \quad \text{for} \quad i = 1, 8 \qquad (1)$$

where λ_i is the wavelength of AIRS channel i, p_k is the pressure level k out of 40 levels, I_m is the measured radiance, I_{clr} and I_{cld} are the computed clear-sky and cloudy (opaque) radiances, respectively.

For the computation of I_{clr} and I_{cld} we need spectral transmissivity profiles corresponding to the observed atmospheric profile as well as spectral surface emissivity. Spectral transmissivity profiles are taken from the Thermodynamic Initial Guess Retrieval (TIGR) dataset (Chédin et al., 1985; Chevallier et al., 1998). They have been computed for the AIRS channels by the Automatized Atmospheric Absorption Atlas (4A) radiative transfer model (Scott and Chédin, 1981) for about 2100 different atmospheric profiles. We compare the observed NASA L2 atmospheric temperature and water

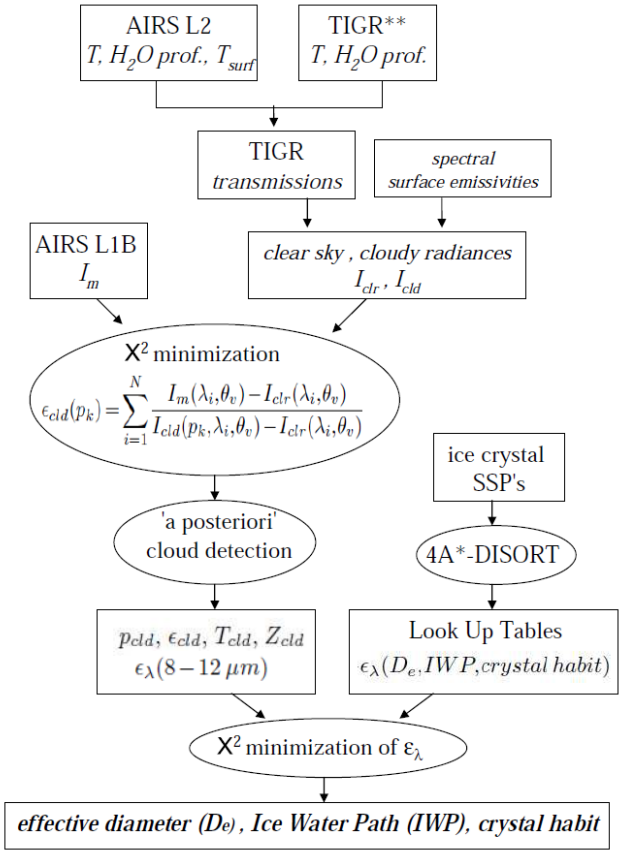

Fig. 1. LMD cloud property retrieval scheme.

vapour profiles to those of the TIGR dataset and choose the spectral transmissivity profiles of the TIGR atmospheric profiles which are the most similar to the observed one, as described in Stubenrauch et al. (2008). Spectral surface emissivities are taken from monthly climatologies using AIRS in the latitude band 30° N–30° S (Péquignot et al., 2008, available at: http://ara.abct.lmd.polytechnique.fr/) and MODIS at higher latitudes (Seemann et al., 2008). The χ^2_w method was developed by Stubenrauch et al. (1999) to take into account (1) the vertical weighting of the different channels, (2) the growing uncertainty in the computation of p_{cld} with increasing p_k and (3) uncertainties in atmospheric profiles. When the χ^2_w method leads to a non-acceptable value of ϵ_{cld} (larger than 1.5, this threshold includes noise for low level clouds), the scene is set to clear-sky (as well as in the case of $\epsilon_{cld} < 0.05$). Cloud temperature T_{cld} is determined from p_{cld}, using the AIRS L2 temperature profile. The cloud property retrieval is applied to all AIRS footprints. The distinction between cloudy-sky and clear-sky is essentially based on the spectral coherence of cloud emissivity in the range 9–11 µm. Therefore the spectral cloud emissivities are determined, as in Eq. (1) by using this time the retrieved cloud pressure. In addition, we determine horizontal scene homogeneity of the 3×3 AIRS footprints per AMSU footprint by using cloud type information (according to p_{cld} and ϵ_{cld}: opaque high clouds, cirrus, thin cirrus, two types of midlevel clouds, two types of low-level clouds and clear-sky). More details can be found in Stubenrauch et al. (2010).

Cloud amount and cloud properties have been evaluated using two years of collocated CALIPSO data (Stubenrauch et al., 2008, 2010): the retrieved AIRS cloud pressure of 72 % of high ($p_{cld} < 440$ hPa) and of 59 % of low-level ($p_{cld} > 680$ hPa) clouds lies within 75 hPa of the "apparent" middle (see Sect. 2.3) of the CALIPSO cloud layers. This means that neither cloud pressure (and deduced cloud temperature) nor cloud emissivity correspond to the top of the cloud, but to a layer within the cloud (Stubenrauch et al., 2010). For this reason, the cloud IR emissivity is often called "effective emissivity" (Pavolonis, 2010), but since the retrieved cloud height is also an "effective" or "radiative" cloud height, we omit these attributes in the following for a more fluid reading.

2.2 AIRS bulk microphysical properties of semi-transparent cirrus

In the following we describe the methodology used to retrieve the D_e and IWP of semi-transparent cirrus (see Fig. 2). The method is based on cirrus spectral emissivity differences in the range 8–12 µm. Cirrus emissivities are determined as in Eq. (1), by using the measured, clear-sky and cloudy spectral radiances. The latter are computed using the retrieved cloud pressure. They are then compared to simulated cirrus emissivities which depend on D_e and IWP. Therefore, cirrus emissivities have been simulated using single scattering properties (SSPs) of column-like or aggregate-like ice crystals. We first describe the simulation of cirrus emissivities and choice of AIRS channels and then the retrieval using a look-up table (LUT) approach.

2.2.1 Simulation of cirrus emissivities

The calculation of the radiative impact of cirrus requires the precise knowledge of the SSPs of ice crystals. SSPs depend on the complex refractive index of the particle, on particle habit as well as on the size parameter (the ratio between the characteristic particle dimension and the incident wavelength). We use a data base of extinction cross section, single scattering albedo and asymmetry parameter determined for column-like and aggregate-like ice crystals provided by MetOffice (Baran et al., 2001; Baran and Francis, 2004). The aspect ratio of the column-like ice crystals decreases with maximum dimension and is constant for aggregate-like ice crystals.

To compute interactions between ice crystals and radiation over an entire population of randomly oriented particles, the SSPs of the individual crystals have been integrated over a bimodal size distribution, with an exponential behaviour for small ice crystals and a Γ distribution for larger ones

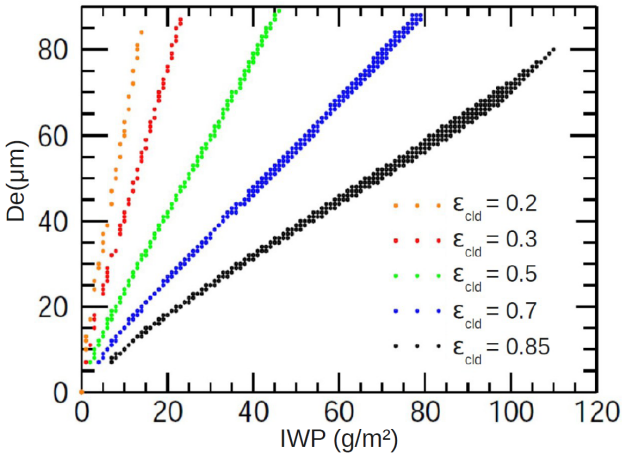

Fig. 2. Effective ice crystal diameter (D_e) as a function of ice water path (IWP) for various simulated cirrus emissivities (ϵ_{cld}) indicated in the legend. Each value of ϵ_{cld} corresponds to the average of an interval of ± 0.05 around this value.

(Mitchell et al., 1996a). This kind of particle size distribution is predicted from growth processes of water vapour deposition and aggregation (e.g. Arnott et al., 1995; McFarquhar and Heymsfield, 1997a) and has been confirmed by in situ measurements (Mitchell et al., 1996a; Mace et al., 1998; Field et al., 2005; Field and Wood, 2007). The PSD used in this study was probably not affected by the shattering problem (Mitchell et al., 2011). The ice crystal population is characterized by its crystal habit and by its ice crystal mean D_e which is considered as an effective photon path through the PSD (before internal reflection takes place). According to McFarquhar and Heymsfield (1997b), Wyser and Yang (1998) and Mitchell (2002), it can be calculated as the ratio of total volume and total orientation-averaged projected area of the entire crystal population as in Eq. (2):

$$D_e = \frac{3}{2} \frac{\int_0^\infty V(r) \cdot n(r) \mathrm{d}r}{\int_0^\infty < P(r) > \cdot n(r) \mathrm{d}r} \quad (2)$$

where V and P are the volume and projected area of an individual ice crystal and $n(r)$ the number of particles with radius r. The SSPs, which are functions of D_e and wavelength, are implemented into the line-by-line 4A radiative transfer model (Scott and Chédin, 1981) which is coupled (Pierangelo et al., 2005) with a multiple scattering model based on discrete ordinate radiative transfer (DISORT, Stamnes et al., 1988). For the simulation of cirrus emissivities we use the same cloud, atmospheric and surface properties as in Rädel et al. (2003): cloud top height is 10 km (corresponding to cloud top temperature of 237 K), cloud vertical extent is 1 km, surface temperature is 300 K, lapse rate is 6.3 K km^{-1} and surface emissivity is set to 1. Section 3 describes sensitivity studies linked to changes in these parameters. Spectral cirrus emissivities are calculated as in Eq. (1), with I_m depending on D_e and IWP. Therefore I_m is simulated by varying D_e from 7 to 85 µm and the IWP varying from 1 to 120 g m^{-2}, separately for two different ice crystal habits (column-like and aggregate-like) and for eight AIRS viewing zenith angles between 0°and 30°. Radiances for clear-sky and for an opaque cloud situated at the same height as the cirrus are also simulated for these eight AIRS viewing zenith angles. These pre-calculated cirrus emissivities at wavelengths between 8 and 12 µm are stored as look-up tables for the retrieval application. We want to point out that by using cirrus emissivities instead of brightness temperatures, the surrounding atmosphere is taken into account (Rädel et al., 2003); therefore, one does not need to produce LUTs for different atmospheres. Figure 2 presents the simulated range of D_e and IWP for a given cirrus emissivity at 12 µm for a cloud composed of aggregate-like ice crystals. From this Figure we first deduce that different couples of D_e and IWP can produce the same cirrus emissivity: small D_e and small IWP to large D_e and large IWP. However, whereas the range of D_e stays the same, the range of IWP increases with increasing cirrus emissivity. Figure 3 presents cirrus spectral emissivity differences, normalized by emissivity at 12 µm, as a function of wavelength, separately for column-like and for aggregate-like ice crystals. Simulations are shown separately for an IWP of 10 g m^{-2} and of 20 g m^{-2}, and each for three values of D_e (10, 30 and 50 µm). We observe that wavelengths between 8 and 10 µm are the most sensitive to the variation of D_e. We also note that the sensitivity to D_e decreases with increasing IWP. It appears that the cirrus emissivity between 8 and 10 µm is also sensitive to crystal habit: aggregate-like ice crystals lead to larger cirrus spectral emissivity differences than column-like ice crystals. The cirrus emissivity range for which a retrieval of D_e is possible has already been explored for TOVS by Rädel et al. (2003). For a given cirrus emissivity at 11 µm (ϵ_{11}), which corresponds to a certain IWP, $\Delta\epsilon_{11-9}$ increases with decreasing D_e. The difference is maximum for a semitransparent cirrus of $\epsilon_{11} \simeq 0.7$ and becomes zero if the emissivity reaches 0 or 1. However, AIRS provides more spectral information than TOVS.

2.2.2 Retrieval

For the retrieval of D_e and IWP we have selected two channels in the range around 9 µm, two channels around the slope between 10 and 11 µm, and the average of two channels around 12 µm (indicated in black in Fig. 3). The selected channels in the 8–12 µm range are those with the weakest absorption lines and smallest noise (by studying the simulated AIRS brightness temperatures of the TIGR dataset). Some channels could not be used, because they were not operational over the whole period (channels 518, 585 and 963), and some channels provide redundant information, so that by using more channels we obtained very similar results. This is in agreement with studies by L'Ecuyer et al., 2006 and Kahn et al., 2008), which have shown that the retrieval does

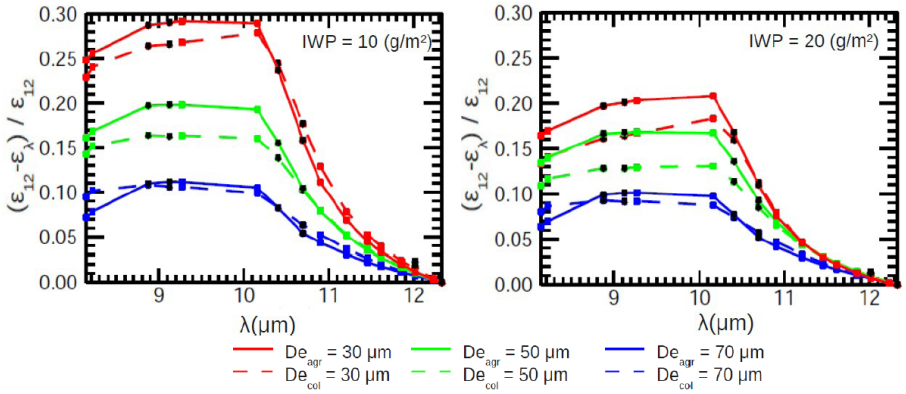

Fig. 3. Cirrus spectral emissivity difference, normalized by cirrus emissivity at 12 µm, as a function of wavelength, separately simulated for aggregate-like and column-like ice crystal habit (full lines and broken lines, respectively). Results are shown for two values of IWP, 10 g m^{-2} (left) and 20 g m^{-2} (right) and for three values of D_e (10, 30, 50 µm, red, green and blue, respectively). The six AIRS channels selected for the retrieval are indicated as black squares.

not improve by adding additional spectral information when the most sensitive channels are already being used. Once the physical cloud properties (p_{cld} and ϵ_{cld}) are determined by the χ^2_w method (see Sect. 2.1 and Fig. 1), cirrus spectral emissivities at 8.87, 9.12, 10.41, 10.70, 12.02 and 12.33 µm (corresponding to AIRS channels 1244, 1185, 903, 835, 557, 502) are determined for high clouds ($p_{cld} < 440$ hPa) according to Eq. (1). I_{cld} is computed by using the retrieved cloud pressure p_{cld}. Then the cirrus emissivities (ϵ^m) are compared to pre-calculated ones which have been stored in LUTs (ϵ^s) as function of D_e and IWP, separately for the two assumed ice crystal habits (column-like or aggregate-like) (see Sect. 2.2.1). We choose for each crystal habit D_e and IWP for which the six simulated cirrus spectral emissivities are the the most similar to the retrieved ones, Eq. (3), where $\sigma(\epsilon^s_\lambda)$ is the root mean square of the spectral variance of the simulated cirrus emissivities:

$$\Delta_{\theta_v}(D_e, IWP) = \frac{\sum_{i=1}^{6}(\epsilon^m_{\lambda_i,\theta_v} - \epsilon^s_{\lambda_i,\theta_v}(D_e, IWP))^2 * \sigma(\epsilon^s_{\lambda_i,\theta_v})}{\sum_{j=1}^{6}\sigma(\epsilon^s_{\lambda_j,\theta_v})} \quad (3)$$

and λ_i representing the i-th channel and θ_v the viewing angle.

2.3 Cloud vertical structure from geometrical profiling CloudSat – CALIPSO data

The lidar CALIOP (Winker et al., 2007, 2009) of the CALIPSO mission provides backscatter profiles at 532 nm and at 1064 nm with a vertical and horizontal resolution of about 30 m and 90 m, respectively. Horizontal sampling is 333 m along the track and the distance between two orbits is about 1000 km. The backscatter ratio helps to distinguish between aerosols and clouds. CALIPSO provides the geometrical height of cloud top and "apparent" cloud base of the cloud layers. It is even sensitive to subvisible cirrus. The "apparent" cloud base is higher than the real cloud base in the case of optically thick clouds for which the lidar signal only penetrates the cloud to an optical depth of up to about 5 (Winker et al., 2003). The 94 GHz nadir-viewing radar CPR (Cloud Profiling Radar) of the CloudSat mission (Stephens et al., 2002) measures profiles of the power backscattered by clouds at a vertical resolution of about 250 m and with a horizontal resolution of about 2.5 km × 1.4 km. The radar is able to probe optically thick cloud layers and therefore provides the correct cloud base. Combining these two instruments has the potential to describe the complete vertical structure of clouds. However, one has to remember that the narrow swath view of these instruments means that they observe only a small fraction of all cloudy scenes. In this study we use the CloudSat Radar-Lidar GEOPROF L2 data (Version 3, Mace et al., 2009) that merge the geometrical profiling of CALIOP and CPR. These data have been collocated with AIRS data and CALIPSO cloud L2 data, averaged over 5 km. The latter provide a cloud feature flag and a flag which informs about the horizontal averaging (<5 km, <20 km or <80 km) necessary to identify the cloud (Winker et al., 2003). We excluded subvisible cirrus by excluding cases in which it was necessary to average over more than 5 km for cloud identification. For the analysis of the vertical structure of semi-transparent high ice clouds, we have verified that the AIRS cloud "radiative" altitude lies between the cloud top and the base altitude determined by the Radar-Lidar GEOPROF sample.

3 Sensitivity studies

For our look-up tables the cirrus spectral emissivities were simulated (Sect. 2.2.1) under certain assumptions about the physical parameters of the cloud as well as about the ice crystals. In this section, we study the uncertainties on the retrieved D_e associated with these assumptions. We assume

the standard conditions for the simulation of ice cloud spectral emissivities:

- vertical extent $Z_{\rm cld} = 1\,{\rm km}$,
- cloud height $h_{\rm cld} = 10\,{\rm km} \leftrightarrow T_{\rm cld} = 237\,{\rm K}$,
- randomly-oriented aggregate-like ice crystals integrated over a bimodal Γ size distribution,
- atmospheric lapse rate of $6.3\,{\rm K\,km^{-1}}$,
- surface temperature $T_{\rm surf} = 300\,{\rm K}$,
- surface emissivity $\epsilon_{\rm surf} = 1$.

To study the impact of changes in these assumptions, we have created for each change discussed in Sects. 3.1 and 3.2 new look-up tables. These have been used instead of the standard look-up tables, and average biases are determined by comparing standard retrieval results over the whole globe with these new results, separately for optically thin cirrus and optically thicker cirrus ($\epsilon_{12} \in [0.3; 0.4]$ and $\epsilon_{12} \in [0.7; 0.8]$), each with two examples of $D_{\rm e}$ (15 µm and 60 µm). The scatter between new and old results provides the noise.

3.1 Sensitivity to atmospheric properties

We have independently made the following changes in the simulations:

- increasing cloud vertical extent by 1 km,
- increasing cloud height by 4 km (corresponding to a decrease of $T_{\rm cld}$ by 27 K),
- increasing atmospheric lapse rate to $11.5\,{\rm K\,km^{-1}}$ and
- decreasing surface temperature by 15 K.

$D_{\rm e}$ and IWP have then been retrieved over the globe by using these new LUTs, and the resulting retrieval differences (corresponding to biases) and standard deviations of the difference distributions (indicating the noise) are compiled in Table 1, for the specific cirrus categories and $D_{\rm e}$ categories. The first column indicates the parameter change, with respect to the standard simulation. The other columns show differences between initially retrieved $D_{\rm e}$ ($D^{\rm std}$) and $D'_{\rm e}$ retrieved using the new parameter, normalized by $D^{\rm std}_{\rm e}$. Results are shown separately for optically thin clouds ($\epsilon_{12\,\mu{\rm m}} \in [0.3$–$0.4]$) and relatively thick clouds ($\epsilon_{12\,\mu{\rm m}} \in [0.7$–$0.8]$) and also for small ($D_{\rm e} \simeq 15$ µm) and large ($D_{\rm e} \simeq 60$ µm) ice clouds. In general, all changes have a small impact on the $D_{\rm e}$ averages (less than 5 %), with an average noise less than 5 %. In addition, we increased the vertical extent to 5 km: the uncertainty remains small for optically thick cirrus ($D'_{\rm e}$ is 1 % smaller than $D^{\rm std}$).

To evaluate the effect of partial coverage, we have an indication of heterogeneity at the spatial resolution of about $45\,{\rm km} \times 45\,{\rm km}$ (AMSU footprint) by first distinguishing overcast scenes (all AIRS footprints cloudy) from partly cloudy scenes. For overcast scenes we distinguish scenes with cirrus only from those mixed with other cloud types (see Sect. 2.1). We assume that heterogeneous scenes have a higher probability for an AIRS footprint to be only partially covered by an ice cloud. The retrieval is therefore applied to overcast cirrus scenes. When including heterogeneous overcast scenes (which add 12 % to the statistics of AMSU footprints that are entirely covered by cirrus), the retrieved $D_{\rm e}$ is on average only 3 % smaller.

However, analyzing partially cloud covered AMSU footprints (with AIRS footprints not surrounded by other cloudy footprints), $D_{\rm e}$ are on average 10 % smaller than the ones determinated for fully covered footprints. On the other hand, the population of cirrus within partially cloud covered AMSU footprints is, on a global scale, 10 times smaller than the population of overcast cirrus. A simulation study by Rädel et al. (2003) has already revealed that partially covered pixels lead to a smaller $D_{\rm e}$.

3.2 Sensitivity to ice crystal properties

Additional sensitivity studies concern other ice crystal habit and approaches to determine the single scattering properties. SSPs by Baran and Francis (2004) have been determined using the T-Matrix computations combined with computations using the Complex Angular Momentum approximation for larger particles. The SSP determination by Mitchell et al. (1996a); Mitchell (2002) is based on the Anomalous Diffraction Approximation. Comparisons by Mitchell et al. (2006) have shown a good agreement between SSPs obtained by both methods. Therefore, only the difference in habit remains: aggregated columns (Baran) compared to aggregated plates (Mitchell). To study the effect on our retrieval, we have simulated cirrus emissivities using SSPs of aggregated plates by Mitchell, integrated over the same crystal size distribution. Resulting differences are again shown in Table 1, for replacing aggregated columns by pristine columns and for replacing aggregated columns by aggregated plates. Mean biases are less than 6 % and the noise is slightly larger when comparing aggregated columns to aggregated plates ($\simeq$10 %). By using LUTs for both, pristine and aggregated columns, the retrieval also provides an estimation of the most probable ice crystal habit. For each retrieval we determine the first and second best fit (minimum Δ in Eq. 3) $D_{\rm e}$ and IWP for each crystal habit, and then we choose the overall best fit. For most of the cases, the first and second best fits of $D_{\rm e}$ stem from the same ice crystal habit (96 % and 87 % for small and large particles, respectively). For these cases the difference between the first and second best solution of the retrieved $D_{\rm e}$ is quite small (within 4 %). When both best fits do not present the same habit (4 % and 13 % for small and large particles, respectively), the difference in the retrieved $D_{\rm e}$ remain small (slightly larger for optically thin clouds). In

Table 1. Compilation of the uncertainties sources and their influence on the retrieval of the mean ice-crystal diameter D_e^{std}. Biases and noise determined as average and standard deviation of $(D_e^{std} - D'_e)/D_e^{std}$ distributions from retrieval statistics over 2 yr. For thin clouds $\epsilon_{cld} \in [0.3, 0.4]$ and for thick clouds $\epsilon_{cld} \in [0.7, 0.8]$. $D_e \simeq 15$ µm corresponds to $D_e \in [10$ µm, 20 µm$]$ and $D_e \simeq 60$ µm corresponds to $D_e \in [50$ µm, 70 µm$]$.

	$(D_e^{std} - D'_e)/D_e^{std}$			
	Thin clouds		Thick clouds	
	15 µm	60 µm	15 µm	60 µm
Vert. ext.: $\Delta Z_{cld} = +1$ km	3 % ±6 %	−1 % ±3 %	2 % ±3 %	−1 % ±3 %
Vert. ext.: $\Delta Z_{cld} = +4$ km	−8 % ±10 %	−1 % ±5 %	2 % ±5 %	−1 % ±5 %
Height: $\Delta h_{cld} = +4$ km	1 % ±4 %	1 % ±2 %	−1 % ±2 %	−1 % ±1 %
Lapse Rate ($6.3 \rightarrow 11.5$ K km^{-1})	2 % ±4 %	−1 % ±3 %	2 % ±3 %	−1 % ±2 %
Surf. temp $\Delta T_s = -15$ K	1 % ±2 %	−2 % ±1 %	1 % ±2 %	−1 % ±1 %
complex habit → pristine habit	−2 % ±5 %	2 % ±5 %	1 % ±4 %	2 % ±5 %
SSP (Baran → Mitchell)	−1 % ±8 %	2 % ±10 %	−1 % ±8 %	1 % ±9 %

this case we choose the average of the two D_e, and the habit is set to uncertain.

4 Retrieval applicability

We apply the retrieval of bulk microphysical properties to all AIRS footprints supposed to be covered by ice clouds. Therefore, we select overcast AMSU footprints, containing high clouds ($p_{cld} < 440$ hPa) with $T_{cld} < 260$ K. The latter threshold corresponds to one for ice clouds in the International Satellite Cloud Climatology Project (ISCCP, Rossow and Schiffer, 1999). Furthermore, we only consider AIRS footprints observed under a zenith viewing angle smaller than 30°(52 % of AIRS fields of view), so that integral product of IWP corresponds closest to the cloud vertical extent. In this section we investigate the relationships between the cirrus bulk microphysical properties and their physical properties.

4.1 Relationship with cloud effective emissivity

From Rädel et al. (2003) we know that the retrieval sensitivity of D_e decreases towards clouds with low and high emissivity. Figure 4 presents retrieved D_e and IWP as well as fraction of aggregate-like ice crystals and the uncertainty in habit as a function of AIRS cloud emissivity determined by the χ^2_w method. Results are shown separately for three latitude bands and two seasons. Abrupt changes in behaviour indicate the range of cloud emissivity in which the bulk microphysical properties are well retrieved: the fraction of uncertain habit (Sect. 3.2) strongly increases in the midlatitudes for cloud emissvity smaller than 0.2 and drops to nearly 0 when $\epsilon_{cld} > 0.85$. The retrieved IWP strongly increases with ϵ_{cld} (and this similarly for all latitude bands and seasons) to reach a maximum at ϵ_{cld} around 0.85. These behaviours indicate that the retrieval of bulk microphysical properties can be conducted for AIRS for ϵ_{cld} between 0.2 and 0.85, corresponding to semi-transparent cirrus. These boundaries are consistent with previous studies (Rädel et al., 2003). The lower emissivity threshold for the TOVS retrieval was fixed at $\epsilon_{cld} = 0.3$, but the improvement of the spectral and spatial resolution of the AIRS instrument allows us to reduce this value to $\epsilon_{cld} = 0.2$. Bulk microphysical properties of these semi-transparent cirrus correspond to an average over the whole cloud vertical extent (Rädel et al., 2003), whereas for optically thick clouds, the instrument only sounds the upper part of the cloud (Sect. 5.2).Within this range, D_e slightly increases with ϵ_{cld}, and the spread between latitudes and seasons is larger than for IWP. The fraction of aggregate-like ice crystals also slightly increases with ϵ_{cld}, reaching 0.6 for $\epsilon_{cld} > 0.55$. The spread between latitude bands and seasons increases towards small ϵ_{cld}, with less complex ice crystal habits for cirrus in Northern Hemisphere (NH) midlatitudes during winter.

4.2 Distinction between ice clouds and mixed phase clouds

Figure 5 presents retrieved D_e and IWP as well as fraction of aggregate-like ice crystals and of column-like crystals as function of AIRS cloud temperature, separately for three latitude bands and two seasons. The sum of the fraction of aggregate-like ice crystals and of column-like crystals is not equal to 1, because for some cases the habit is set to uncertain (Sect. 3.2). On the figure we distinguish two regimes:

– $T_{cld} < 230$ K: D_e and IWP increase with increasing T_{cld} and the fraction of aggregate-like ice crystals ($\simeq 0.6$) remains approximately constant.

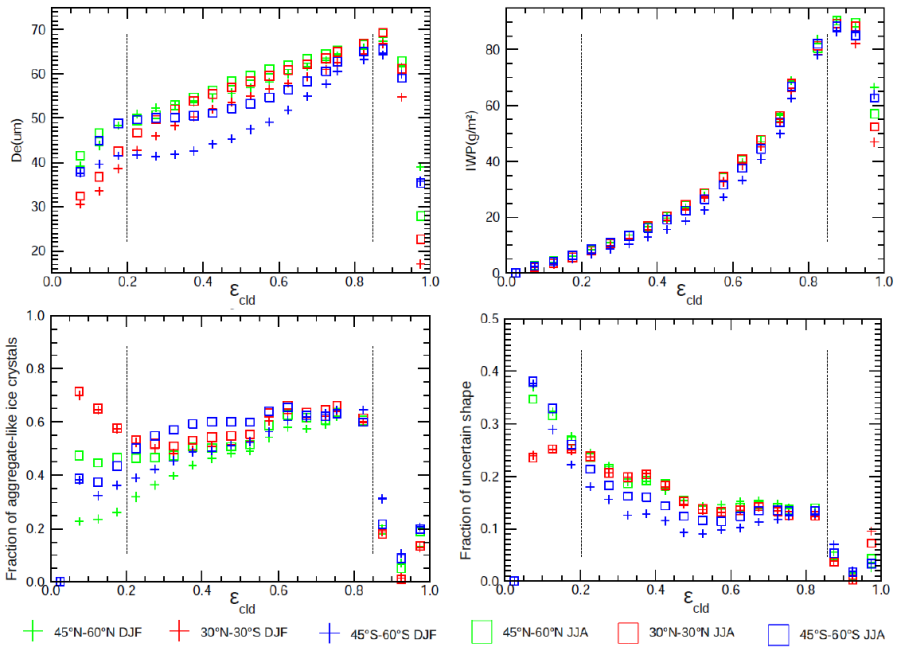

Fig. 4. Bulk microphysical properties as function of cloud emissivity, averaged over the period 2003–2009. Crosses and squares represent averages over boreal winter and over boreal summer, respectively. Green symbols are for NH midlatitudes, red for the tropics and blue for SH midlatitudes. The vertical lines represent the emissivity boundaries between which the microphysical property retrieval is applied.

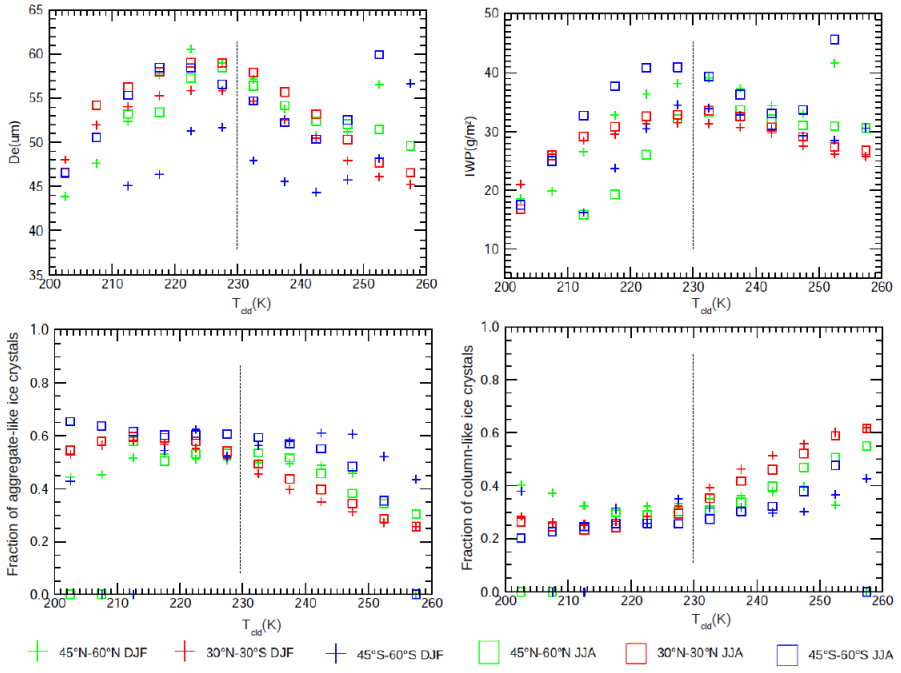

Fig. 5. Bulk microphysical properties as function of cloud temperature, averaged over the period 2003–2009. Crosses and squares represent averages over boreal winter and over boreal summer, respectively. Green symbols are for NH midlatitudes, red for the tropics and blue for SH midlatitudes. The vertical line at $T_{\mathrm{cld}} = 230\,\mathrm{K}$ represents the temperature threshold below which the microphysical property retieval is applied.

Table 2. Fraction of high clouds kept within cloud emissivity and cloud temperature boudaries for three latitude bands (NH:45° N–60° N, Trop: 15° N–15° S, SH: 45° S–60° S), for boreal winter and boreal summer and over ocean and land separately.

	Ocean		Land		All	
	DJF	JJA	DJF	JJA	DJF	JJA
$0.2 \leq \epsilon_{cld} \leq 0.85$						
NH midlatitudes	70 %	69 %	79 %	69 %	73 %	69 %
Tropics	66 %	67 %	71 %	70 %	68 %	68 %
SH midlatitudes	64 %	73 %	74 %	75 %	64 %	73 %
$T_{cld} \leq 230$ K						
NH midlatitudes	63 %	18 %	59 %	28 %	62 %	23 %
Tropics	59 %	55 %	46 %	41 %	55 %	51 %
SH midlatitudes	20 %	66 %	42 %	73 %	21 %	66 %

– $T_{cld} > 230$ K: D_e and IWP decrease with increasing T_{cld} and the fraction of column-like ice crystals strongly increases with increasing T_{cld}

The change in behaviour of D_e and IWP around 230 K as well as the increase of the rate of column-like ice crystals (with SSPs more similar to spheres than to aggregate-like ice crystals) demonstrate that clouds with T_{cld} between 230 and 260 K may include a substantial part of water droplets which influence the retrieval. Thus pure ice clouds preferably occur when $T_{cld} < 230$ K. This is in agreement with previous studies (Yang et al., 2002; Hu and Winker, 2009; Riedi et al., 2010; Martins et al., 2011). Cloud temperature does not much affect the crystal habit in pure ice clouds, which is consistent with the fact that the aspect ratio of small particles is a weak function of temperature (Korolev and Isaac, 2003).

4.3 Occurrence of semi-transparent high ice clouds

From the findings in Sects. 4.1 and 4.2 we define Semi-Transparent Cirrus, referenced as ST-HIC, as:

$$\begin{aligned} \text{high clouds:} &\quad p_{cld} \leq 440\,\text{hPa} \\ \text{pure ice clouds:} &\quad T_{cld} \leq 230\,\text{K} \\ \text{semi-transparent clouds:} &\quad 0.2 \leq \epsilon_{cld} \leq 0.85 \\ \text{(corresponding to visible optical depth:} &\quad 0.4 \leq \tau_{vis} \leq 3.8\text{)} \end{aligned}$$

We deduce from Table 2 that about 70 % of all high clouds belong to the semi-transparent cloud category, keeping slightly more clouds in winter. Considering the ϵ_{cld} distributions of ST-HICs in Fig. 6, they are rather flat, with a peak towards large ϵ_{cld} in the midlatitudes, especially in winter. The seasonal variation is stronger in the NH, where the distribution in summer is similar to the ones in the tropics (with more cirrus at low ϵ_{cld}). This may be linked to the fact that over the ocean band in the Southern Hemisphere (SH) midlatitudes storms may also develop in summer. Figure 7 presents frequency distributions of T_{cld}, in NH midlatitudes, the tropics and SH midlatitudes, separately in boreal winter and in boreal summer. We recognize a strong summer-winter difference in the midlatitudes: more than 60 % of semitransparent cirrus present a temperature lower than 230 K in winter and only less than 20 % in summer. From Table 2 we deduce that the seasonal difference is stronger over ocean than over land. In the tropics the frequency distribution is much broader and does not show a seasonal variation in the tropics (with a frequency of 55 %). Figure 8 presents geographical maps of high cloud amount, of semi-transparent high cloud amount and of semi-transparent high ice cloud amount, all relative to total cloud amount, separately for boreal winter (December, January and February) and for boreal summer (June, July and August). Averages correspond to the period 2003–2009. Whereas many of the uppermost clouds in the tropics are semi-transparent high ice clouds, a large fraction of high clouds in the NH midlatitudes over land are also semi-transparent, but also includes liquid droplets in summer. In the SH midlatitudes we observe a small fraction of ST-HICs only in winter. Associated statistics is summarized in Table 3. ST-HICs correspond to about 15 % of all clouds and to about 25 % of high clouds in the tropics, with almost no difference between ocean and land. In the midlatitudes, ST-HICs occur mostly during winter where they represent practically 30 % of high clouds, with a higher occurrence over land.

5 Analysis of D_e, IWP and ice crystal habit

5.1 Geographical and seasonal variations

Figure 9 presents geographical maps of mean IWP and D_e as well as dominating ice crystal habit, separately for boreal winter and for boreal summer. As cloud emissivity (not shown) and IWP, the average D_e is larger in winter than in summer in the midlatitudes. The ice crystal habit is defined as dominating, when one habit appears 10 % more often

Table 3. Amount of high clouds (HC) and semi-transparent high ice clouds (ST-HIC) relative to total cloud amount, averaged over the period 2003–2009 in three latitude bands (NH: 45° N–60° N, Trop: 15° N–15° S, SH: 45° S–60° S), for boreal winter and boreal summer and over different surfaces (ocean, land and all surfaces).

	Ocean		Land		All	
	DJF	JJA	DJF	JJA	DJF	JJA
High Clouds (HC)						
NH midlatitudes	26 %	26 %	43 %	37 %	29 %	32 %
Tropics	64 %	59 %	70 %	62 %	65 %	60 %
SH midlatitudes	10 %	25 %	29 %	51 %	11 %	25 %
Semi-Transparent High Ice Clouds (ST-HIC)						
NH midlatitudes	7 %	1 %	15 %	3 %	9 %	2 %
Tropics	18 %	15 %	16 %	12 %	17 %	15 %
SH midlatitudes	1 %	8 %	5 %	19 %	1 %	8 %

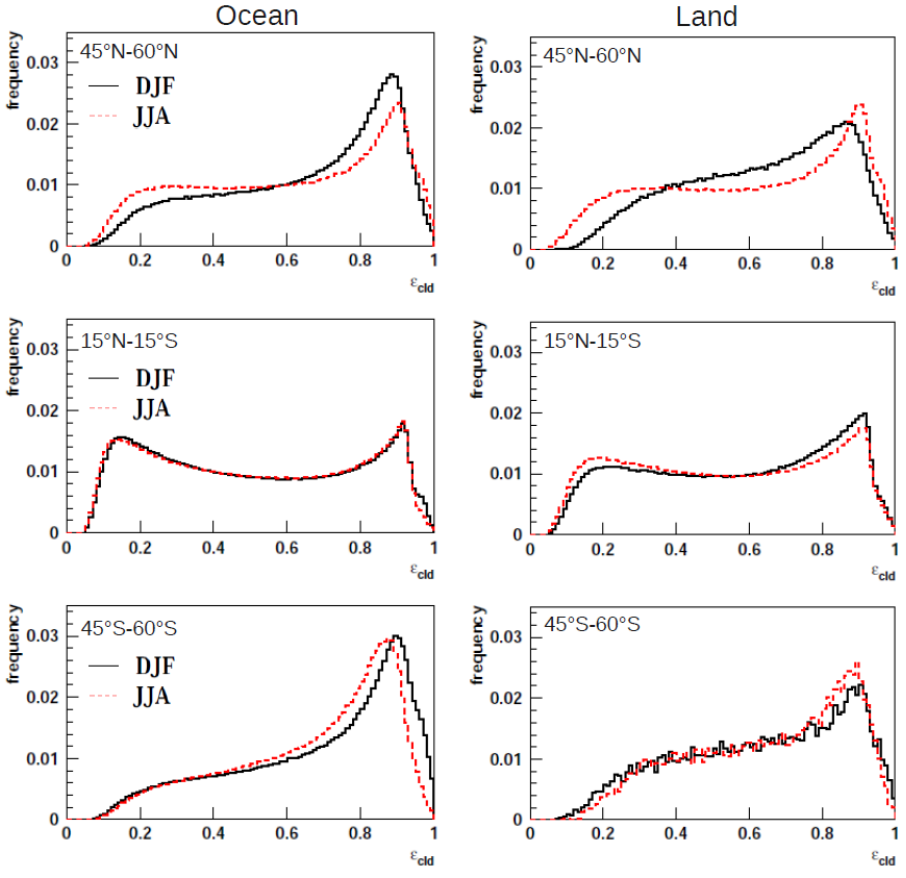

Fig. 6. Normalized frequency distributions of high cloud emissivity over ocean (left) and over land (right), separately for three latitude bands. Boreal winter and boreal summer are represented with black and red lines, respectively. Statistics is over the period 2003–2009.

than the other over the period, otherwise it is set to mixed habit. Furthermore, when no distinction was possible between aggregate-like and column-like ice crystals in more than 40 % of the cases within the grid cell, the dominating habit was set to uncertain. According to Table 4, the fraction of ice clouds containing aggregate-like ice crystal habit is about 50–60 % over ocean and about 40–50 % over land, respectively. As already deduced from Figs. 4 and 5, ST-HICs seem to consist slightly more often of aggregate-like ice crystals. This is consistent with in situ measurements

Table 4. ST-HIC means of physical properties and medians of bulk microphysical properties over the period 2003–2009, in three latitude bands (NH: 45° N–60° N, Trop: 15° N–15° S, SH: 45° S–60° S), for boreal winter and boreal summer and over ocean and land.

	ϵ_{cld}		T_{cld} (K)		ΔZ (km)		% SL		D_e(μm)		IWP (g m^{-2})		Agg(%)		% $D_>85\mu m$	
	DJF	JJA	DJF	JJA	DJF	JJA	DJF	JJA	DJF	JJA	DJF	JJA	DJF	JJA	DJF	JJA
Ocean																
NH midlatitudes	0.57	0.47	222	224	5.5	3.9	52	41	57	54	26	16	50	53	15	5
Tropics	0.49	0.49	217	217	4.9	4.5	50	48	51	54	19	20	56	56	2	4
SH midlatitudes	0.57	0.61	225	221	5.1	6.0	48	49	46	54	18	30	56	62	4	10
Land																
NH midlatitudes	0.57	0.51	220	223	5.5	3.8	67	62	50	53	23	18	41	39	3	1
Tropics	0.52	050	218	218	5.1	4.3	51	48	52	53	21	20	44	45	2	2
SH midlatitudes	0.57	0.58	221	219	3.7	3.2	76	58	29	44	13	20	53	46	1	2
All																
NH midlatitudes	0.57	0.49	221	224	5.5	3.8	62	55	54	53	25	17	48	44	12	5
Tropics	0.50	0.49	217	217	4.9	4.5	50	48	51	54	19	20	53	54	3	4
SH midlatitudes	0.57	0.61	224	221	5.0	5.9	49	49	45	54	18	30	56	61	4	10

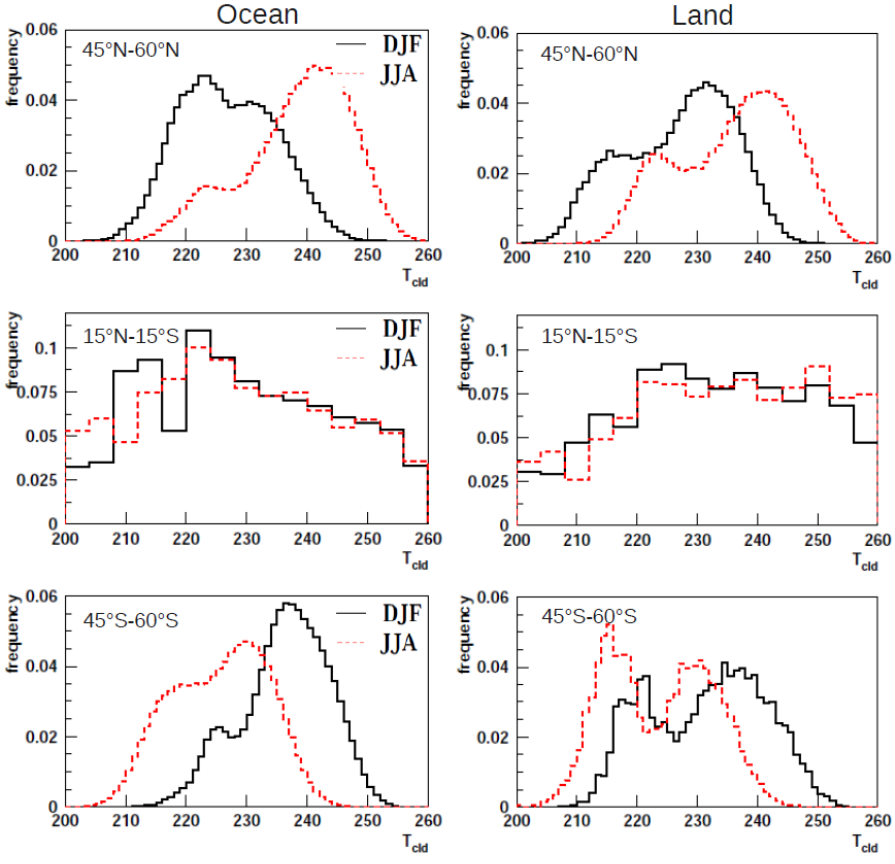

Fig. 7. Normalized frequency distributions of high cloud temperature (in Kelvin) over ocean (left) and over land (right), separately for three latitude bands. Boreal winter and boreal summer are represented with black and red lines, respectively. Statistics is over the period 2003–2009.

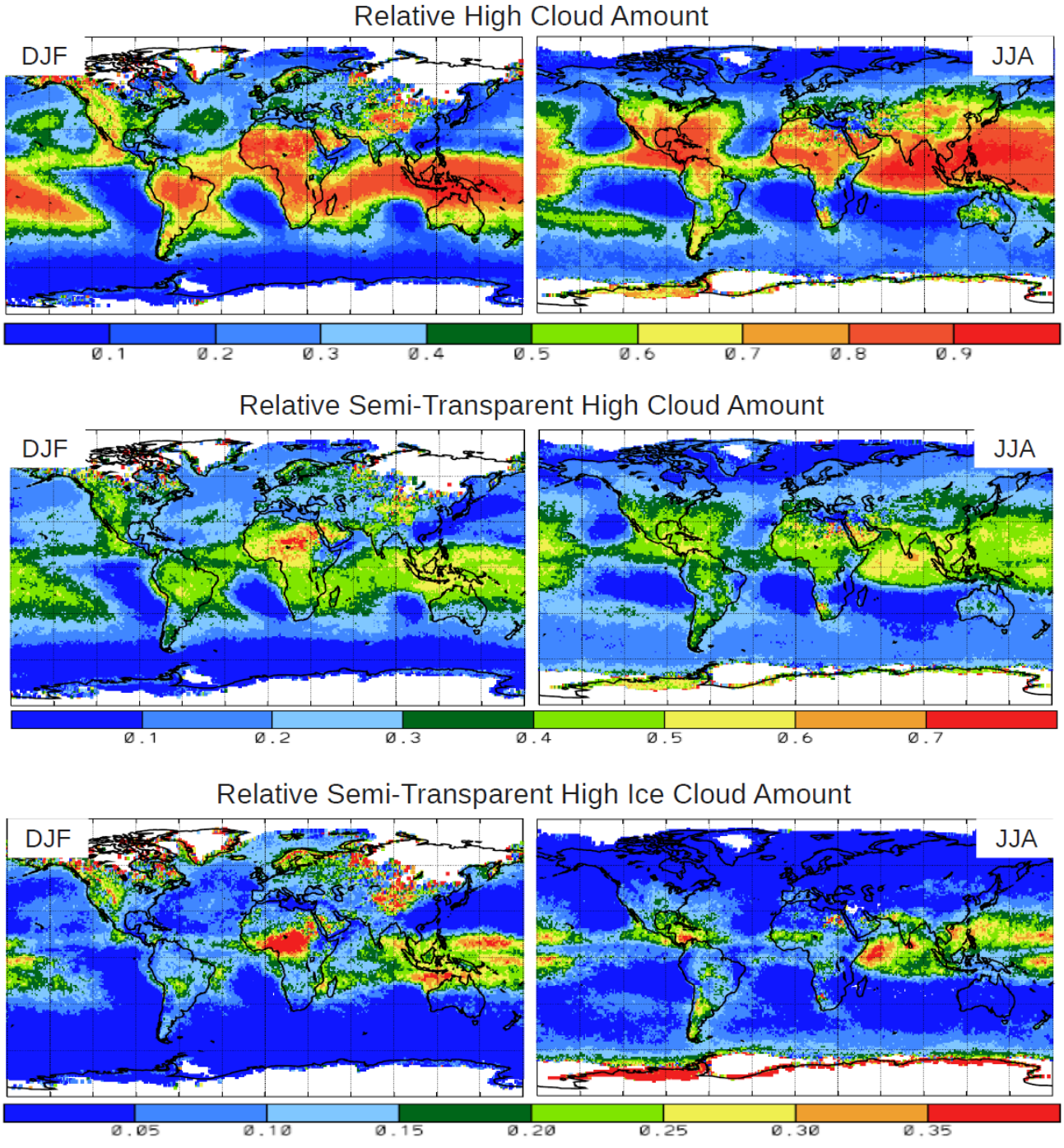

Fig. 8. Geographical maps of high cloud amount (top), semi-transparent high cloud amount (middle) and of semi-transparent high ice cloud amount (bottom), relative to total cloud amount, for boreal winter (right) and boreal summer (left). Statistics is averaged over the period 2003–2009.

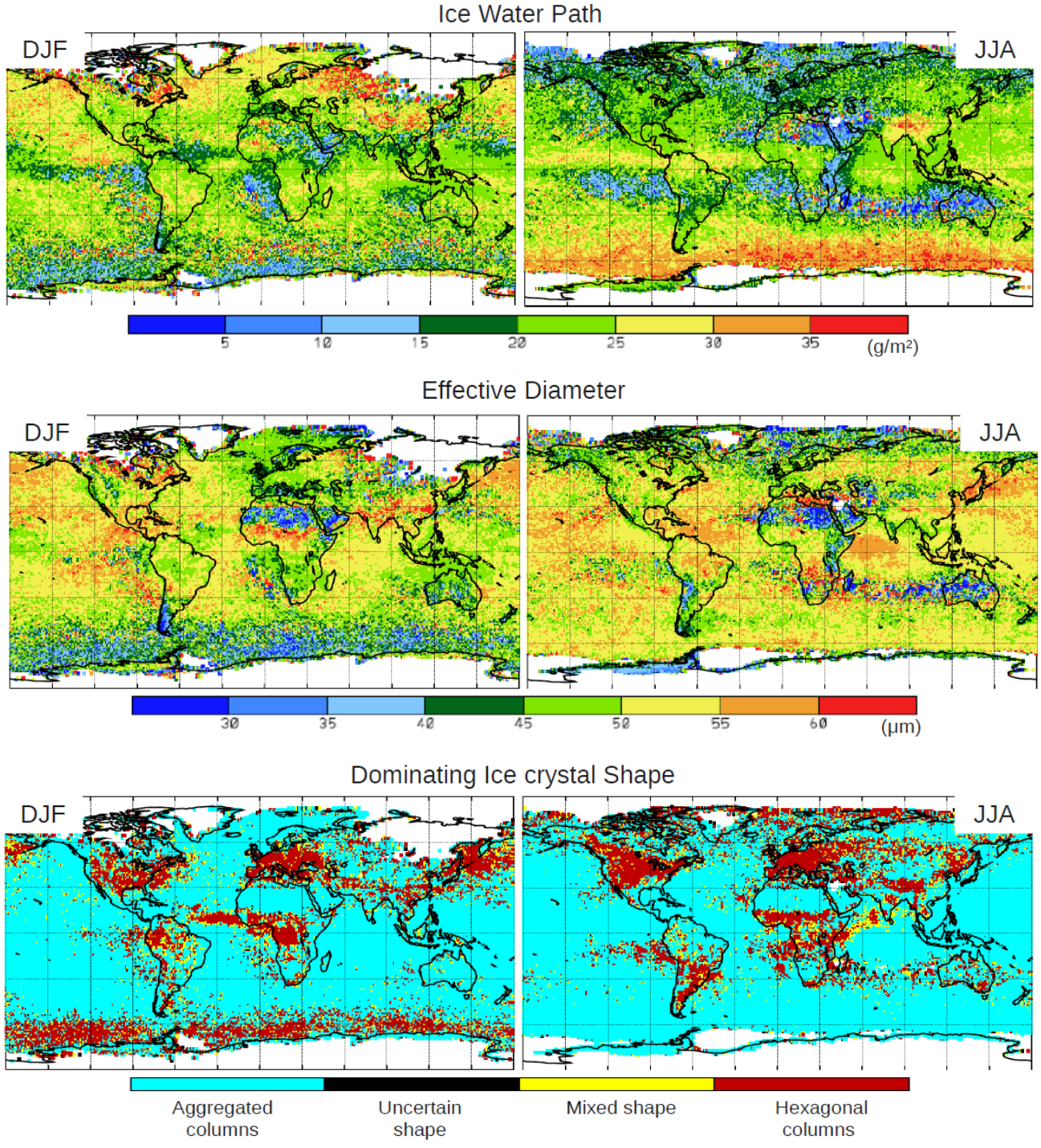

Fig. 9. Geographical maps of ice water path (top), effective ice crystal diameter (middle) and of dominating (occurrence larger than 40 %) ice crystal habit (bottom), for boreal winter (left) and boreal summer (left). Statistics is averaged over the period 2003–2009.

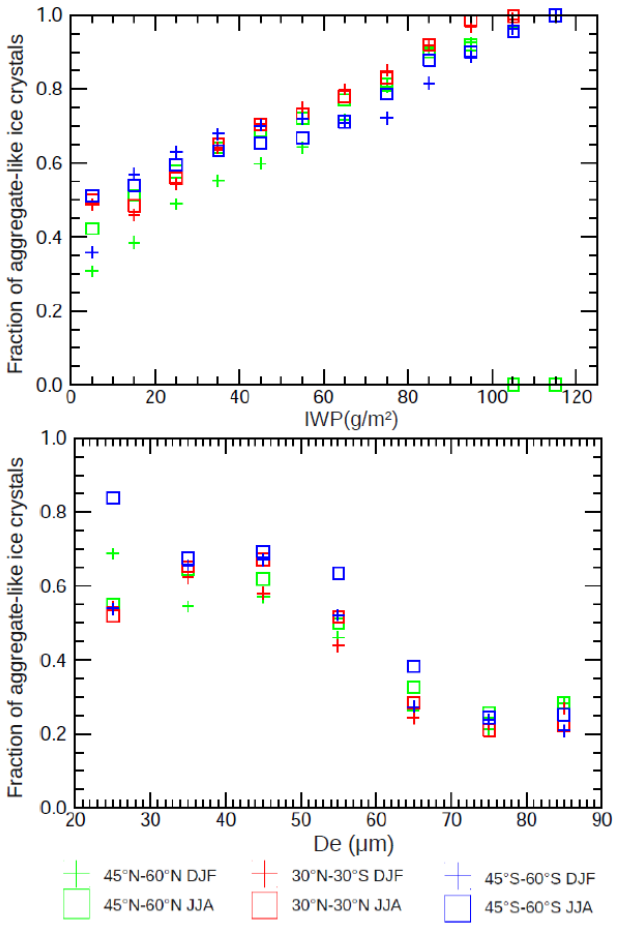

Fig. 10. Relationships between fraction of aggregated-like ice crystals and IWP (top) and between fraction of aggregated-like ice crystals and D_e (bottom) over ocean, separately for boreal winter (+ signs) and for boreal summer (squares). Green symbols are for NH midlatitudes, red for the tropics and blue for SH midlatitudes. Statistics is averaged over the period 2003–2009.

that suggest that irregular is the dominant habit of ice particle grown in natural clouds (e.g. Francis et al., 1999; Korolev and Isaac, 2003; Gayet et al., 2011). Considering Fig. 9, in the SH midlatitudes during summer, in the Northern West Pacific and generally over land ST-HICs seem to be more often composed of column-like ice crystals. Figure 10 reveals that the fraction aggregate-like ice crystals increases with IWP, thus explaining the higher frequency of this habit in the midlatitudes during winter and the higher frequency of column-like ice crystals over land, where ST-HICs have a slightly smaller IWP, especially in summer. This is in agreement with a study by Stubenrauch et al. (2007) which has revealed that aggregate-like ice crystals are more probable for ST-HICs with larger IWP. For a fixed IWP, the fraction of aggregate-like ice crystals decreases with increasing D_e. This is consistent with in situ measurements that show that the habit of ice crystals becomes less spherical as its size increases (Mitchell, 2009). Figure 11 presents normalized frequency distributions of D_e and IWP for NH midlatitudes, tropics and SH midlatitudes, separately for boreal summer and for boreal winter. Whereas D_e distributions are nearly Gaussian, IWP distributions have a long tail towards larger values. In general, less than 5 % of the ST-HICs have a D_e which is larger than the retrieval sensitivity (>85µm), with 10 to 15 % over ocean in winter (Table 4). Therefore we present in Table 4 for bulk microphysical properties median values instead of mean values. They are about 10 % smaller than the corresponding mean values. The IWP distributions reflect the seasonal variation of IWP in the midlatitudes, with larger values in winter. It is interesting to note that the D_e distribution in the SH midlatitudes is also shifted towards larger values.

5.2 Relationship with cloud vertical structure

The Radar-Lidar GEOPROF data, collocated with AIRS data over two years, allow us to characterize the vertical structure of the ST-HICs. Figure 12 presents the normalized frequency distributions of ST-HIC vertical extent separately for boreal winter and for boreal summer for ocean and land in the three latitude bands. The peak values lie around 2.5 km in the midlatitudes, with a slight shift towards larger values in winter, and around 3.5 km in the tropics. Winter midlatitude and tropical distributions are similar, because of occurrence of frontal systems and of convection, both leading to more vertically extended cloud systems. Table 4 summarizes these averages, separately for ocean and land in the three latitude bands. In general, we observe less single layer ST-HICs in the tropics and in the case of winter storm tracks in the midlatitudes and more single layer ST-HICs over land, especially in the midlatitudes. Single layer ST-HICs also largely dominate over the Sahara. We have also studied frequency distributions of D_e and IWP separately for single and multi layer cloud systems (not shown).Distributions are very similar. To explore a possible relationship, Fig. 13 presents average cloud emissivity, D_e, IWP and fraction of aggregated ice crystals for ST-HICs as function of cloud vertical extent, separately over ocean and over land for the three latitude bands and two seasons. In general, emissivity and IWP of ST-HICs increase with vertical extent, once their extent is larger than 2 km. The behaviour is similar over ocean and over land. However, at the same vertical extent, emissivity and IWP of ST-HICs are largest in the SH midlatitudes and smallest in the tropics. This is probably linked to the different types of cirrus, those from anvils in the tropics and those from storms in the midlatitudes. The spread in IWP is less pronounced. D_e and fraction of aggregated ice crystals do not show a dependency on ST-HIC vertical extent, with exception for ST-HICs in summer over land in the NH midlatitudes. At the same vertical extent, D_e in summer over the SH midlatitudes is on average slightly smaller than in the other regions.

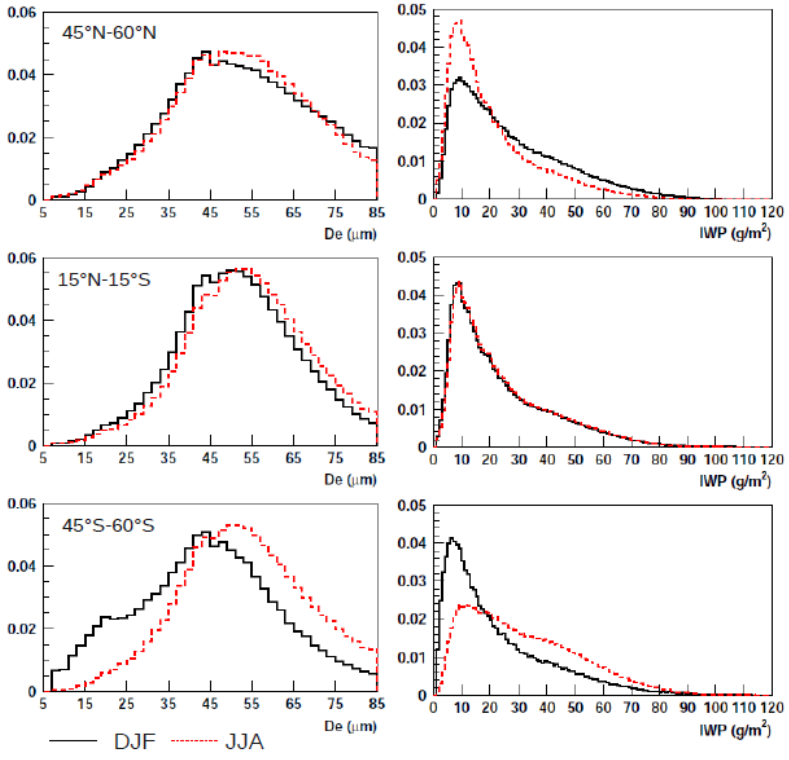

Fig. 11. Normalized frequency distributions of D_e (left) and IWP (right) of ST-HICs for three latitude bands. Boreal winter and boreal summer are represented with black and red lines, respectively. Statistics is over the period 2003–2009.

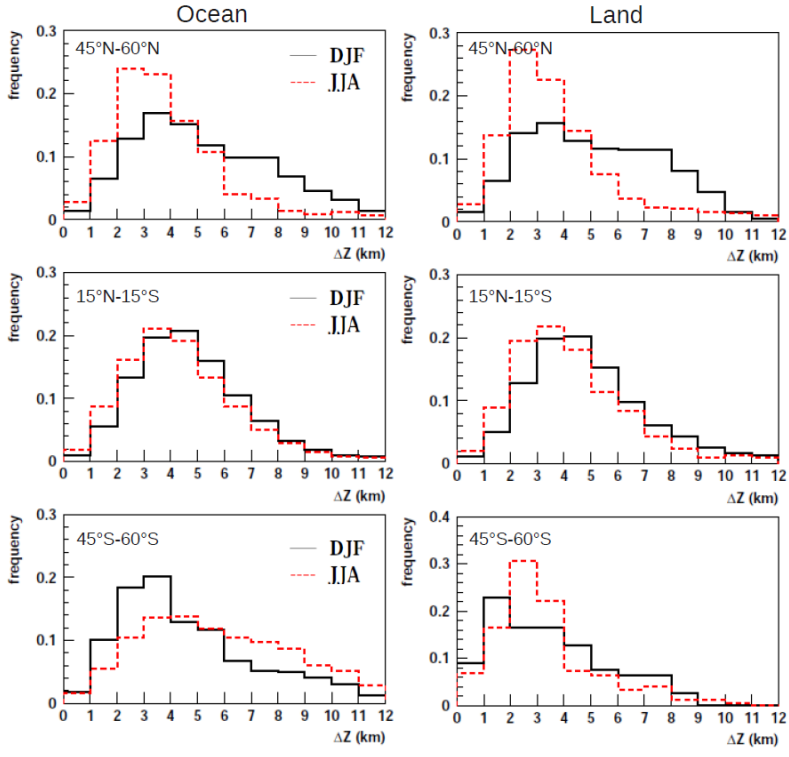

Fig. 12. Normalized frequency distributions of vertical extent of ST-HICs for three latitude bands. Boreal winter and boreal summer are represented with black and red lines, respectively. Statistics is over the period 2007–2008.

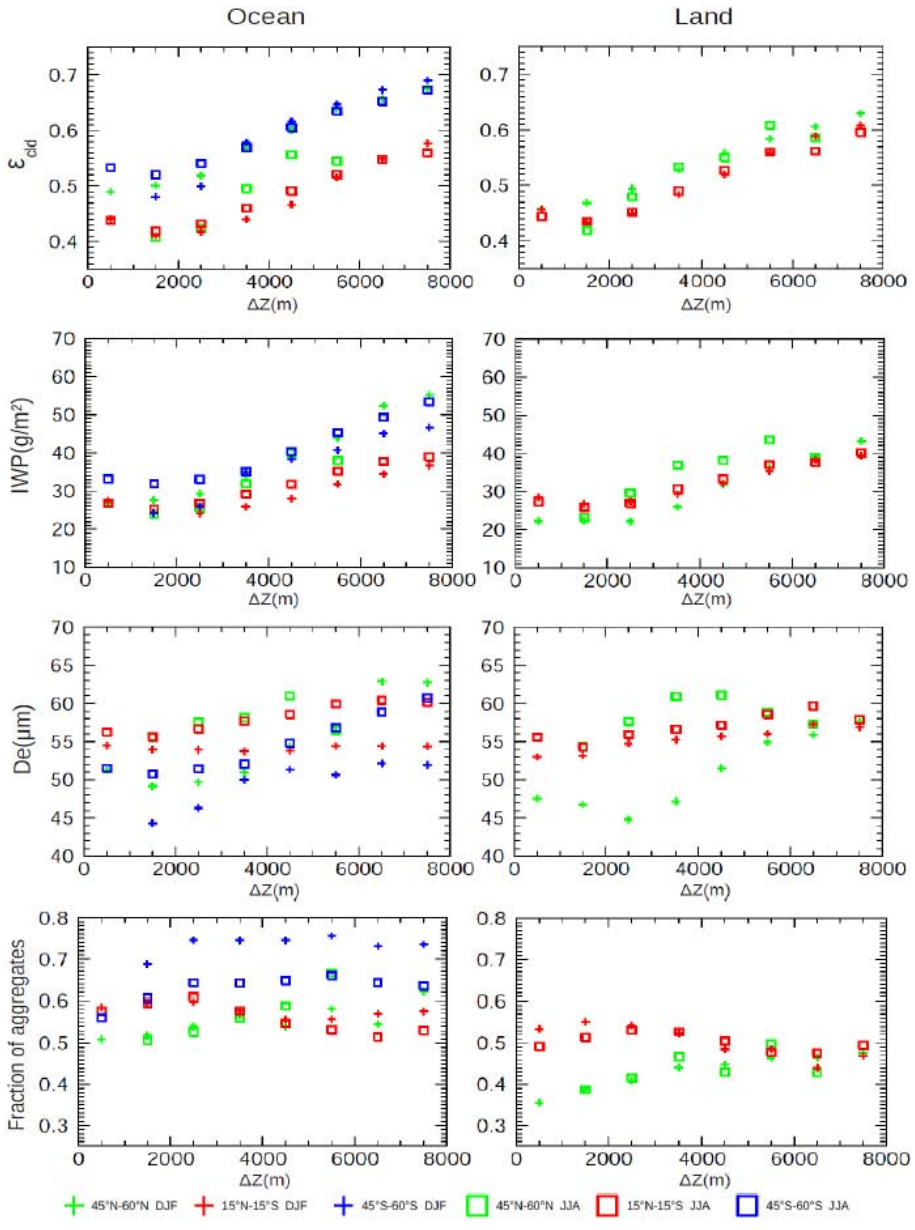

Fig. 13. Relationships between microphysical properties and vertical extent, separately over ocean (left) and over land (right). Green, red and blue signs stand for NH midlatitudes, tropics and SH midlatitudes, respectively. Plus signs and squares indicate boreal winter and boreal summer, respectively.

5.3 Comparison with TOVS

Bulk microphysical properties of semi-transparent cirrus have already been retrieved with TOVS (Stubenrauch et al., 1999, 2004; Rädel et al., 2003), using a similar methodology. Compared to the AIRS retrieval presented in this article, we summarize the following main differences in the TOVS retrievals: single scattering properties have been determined by assuming ice crystals as aggregated plates (Mitchell et al., 1996a); only two channels (at 8.3 and 11.9 µm) were available and therefore first D_e (using LUTs depending on ϵ_{cld} at 8.3 and 11.9 µm) and in a second step IWP (using LUTs depending on D_e and ϵ_{11}) were retrieved; semi-transparent cirrus were defined as $0.3 < \epsilon_{cld} < 0.85$ with $T_{cld} < 260$ K; retrievals are available over the period 1989–1990. Another important difference is the spatial resolution of the retrievals: 100 km for TOVS compared to 13.5 km for AIRS. In Fig. 14, we compare global annual normalized frequency distributions of D_e and IWP from TOVS (in black) and AIRS (in green), separately for three intervals with increasing cloud emissivity and at last for the emissivity intervals for which

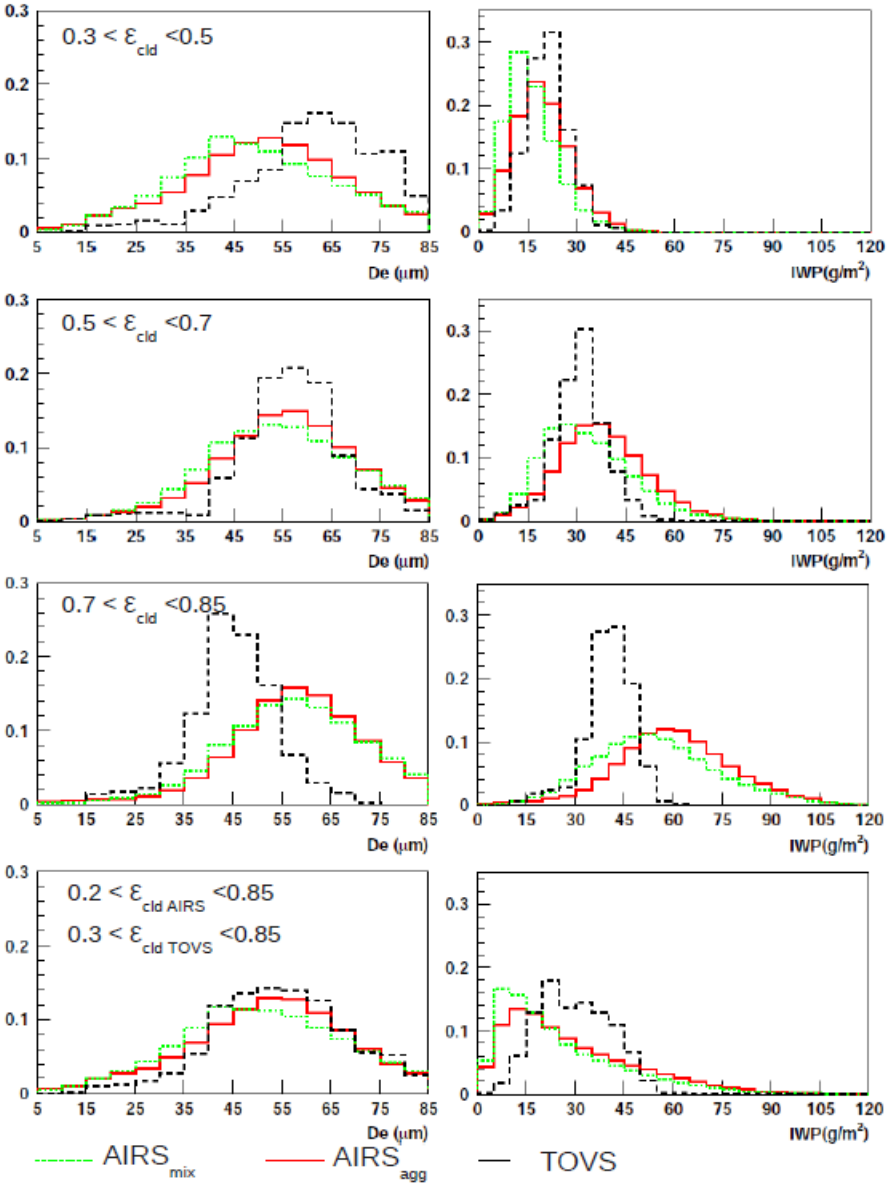

Fig. 14. Normalized frequency distributions of D_e (left) and IWP (right) retrieved from TOVS (dashed black lines) and from AIRS observations (dotted green), separately for different cirrus emissivity intervals. Statistics is over 1987–1990 and 2003–2009, respectively. In addition, the AIRS retrieval has been performed with only two channels and using the same single scattering properties as in the TOVS retrieval (full red lines).

the retrievals are valid. For this comparison we consider clouds with $T_{cld} < 230$ K. In addition, we have included results (in red) from an AIRS retrieval we have performed by using only two channels (channels 557 and 1244) similar to those in TOVS and using the same single scattering properties in the simulation (Mitchell et al., 1996a) as for the TOVS retrieval. In general, the overall distributions (lowest panel) agree quite well, with a slightly wider IWP distribution from AIRS.

Considering the different cirrus emissivity intervals, we observe that both instruments provide very similar D_e and IWP results for ϵ_{cld} between 0.5 and 0.7, which corresponds to the range of maximum sensitivity (Fig. 1 of Rädel et al., 2003). Differences appear when considering smaller and larger cirrus emissivities, larger D_e and smaller D_e and IWP obtained by TOVS. Assuming that the better spectral and spatial resolution of AIRS has led to improvements in the retrieval, a slight overestimation of D_e by TOVS for clouds with small emissivity could be explained by partial cloud cover or spatial heterogeneity (Table 1 of Rädel et al., 2003). The better spectral resolution and the additional channels at wavelengths greater than 8.3 µm of AIRS lead to a slightly

deeper sounding (see Fig. 8 of Rädel et al., 2003), which in the case of optically thicker clouds (see Fig. 14) leads therefore to larger D_e (if one assumes that D_e increases from cloud top to cloud base due to aggregation). From Fig. 14, we also recognize that IWP increases with ϵ_{cld}. The increase is stronger by using AIRS than by using TOVS. This is because D_e obtained from AIRS also increases with ϵ_{cld}. Moreover, the IWP distributions from AIRS become wider, whereas those from TOVS stay quite narrow. This is probably due to the fact that the TOVS two channel method first determines D_e and then IWP from D_e and ϵ_{cld}, whereas the AIRS multi-channel method extracts D_e and IWP simultaneously.

5.4 D_e parameterization

As mentioned in the introduction, cirrus bulk microphysical properties depend on many environmental factors. However, for modelling cirrus radiative effects in GCMs, D_e has to be predicted from other variables. Simple relationships between temperature, ice water content and D_e have been suggested (Kristjansson et al., 2000; Ou et al. (1995); Donovan and van Lammeren, 2002). Our global data set allows us to examine such relationships and to verify if a global parameterization may be found suitable for GCMs. Figure 15 presents the correlation between D_e and IWP, separately for the three latitude bands. For each latitude band we consider three cloud temperature intervals. D_e increases with IWP, a relationship already revealed by different field campaigns (Mitchell et al., 1996a; Korolev et al., 2001). We recognize a rapid growth of D_e for IWP smaller than about 20 g m^{-2}. For larger IWP values, the increase becomes weaker. However, the increase is stronger compared to the studies cited above and to a study by Stubenrauch et al. (2007) using collocated Scanner of Radiation Balance (ScaRaB) and TOVS data. The latter difference in behaviour may be explained by the deeper sounding of AIRS in the case of optically thicker cirrus (see Sect. 5.3) and also by considering only pure ice clouds (since D_e may be smaller for $T_{cld} > 230$ K, see Fig. 5). The parameterization of D_e as a function of IWP that leads to a best fit of these global data (full black line) is described by the expression:

$$D_e(\mathrm{IWP}) = \sum_{i=0}^{4} \alpha_i \cdot \ln(\mathrm{IWP})^i \quad (4)$$

with $\alpha_0 = 9.945$, $\alpha_1 = -11.245$, $\alpha_2 = 27.426$, $\alpha_3 = -9.192$ and $\alpha_4 = 0.974$.

We studied the robustness of the parameterization by randomly separating the data set into two halves and refitting the data again. The coefficients were stable within 0.005. For a fixed IWP, when considering different latitude bands and cloud temperature intervals, the overall spread of D_e is about 10 %. This indicates that D_e depends strongly on IWP (which itself is also related to cloud temperature as shown in Fig. 5), and only slightly directly on cloud temperature. For ST-HICs with the same IWP, we recognize even a different behaviour of D_e with T_{cld}: it increases in the tropics whereas it decreases in the midlatitudes. Previous studies (Ivanova et al., 2001; Boudala et al., 2002; Edwards et al., 2007) used the temperature to parameterize D_e. We found that these parameterizations, generally established for clouds warmer than 230 K, underestimate D_e by about 10 to 20 µm compared to our data (not shown). D_e only varies by about 15 µm within the temperature range between 200 and 230 K (see also Fig. 5), another sign that the dependence on IWP is better suited to parameterize D_e (Baran et al., 2009). Compared to a parameterization developed for in situ measurements at a specific latitude band as for example by Boudala et al. (2002), it seems to be difficult to determine a global multivariate parameterization for D_e dependent on both IWP and temperature, because the latter is not independant as can be seen in Fig. 5. Liou et al. (2008) developed a similar parameterization by using in situ data. They distinguished between warm and cold cirrus, the latters corresponding to our cases. Since field experiments present D_e parameterized as a function of ice water content (IWC) (references above) and IR sounders only provide the integrated IWC (corresponding to IWP), we make use of the synergy with radar-lidar GEOPROF data to provide an estimation of IWC. Therefore, we determine IWC as the ratio between IWP and the vertical extent of the cloud layer, by assuming a vertically constant IWC. This assumption is only realistic for cirrus with a relatively small vertical extent (Seo and Liu, 2006). Figure 16 presents the relationship between D_e and IWC, separately for the three latitude bands in boreal winter and summer. We consider ST-HICs with a vertical extent between 0.5 and 1 km and between 0.5 and 2 km. The statistics of two years is not sufficient to separate into different temperature intervals. D_e also increases logarithmically with IWC, in agreement with different field campaigns (Korolev et al., 2001; McFarquhar et al., 2003; Heymsfield, 2003; Garrett et al., 2004). However, the increase seems to be smaller for larger IWC values than the one for large IWP in Fig. 15. This could be explained by the fact that only ST-HICs with a relatively small vertical extent are considered. We deduce further from Fig. 16 that for cirrus with low IWC, D_e increases more strongly for geometrically thicker clouds than for geometrically thinner clouds. The parametrization of D_e as a function of IWC that leads to a best fit of these global data is described by the equation:

$$D_e(\mathrm{IWC}) = \sum_{i=0}^{2} \alpha_i \cdot \ln(\mathrm{IWC})^i \quad (5)$$

with the following parameters for different vertical extents:

$\Delta Z < 1$ km: $\alpha_0 = 92.608$ $\alpha_1 = 16.544$, $\alpha_2 = -5.126$

$\Delta Z < 2$ km: $\alpha_0 = 83.582$, $\alpha_1 = 3.981$, $\alpha_2 = -6.319$

Some GCMs use a parameterization of D_e as a function of IWC (McFarlane et al., 1992; Liou et al., 2008) at

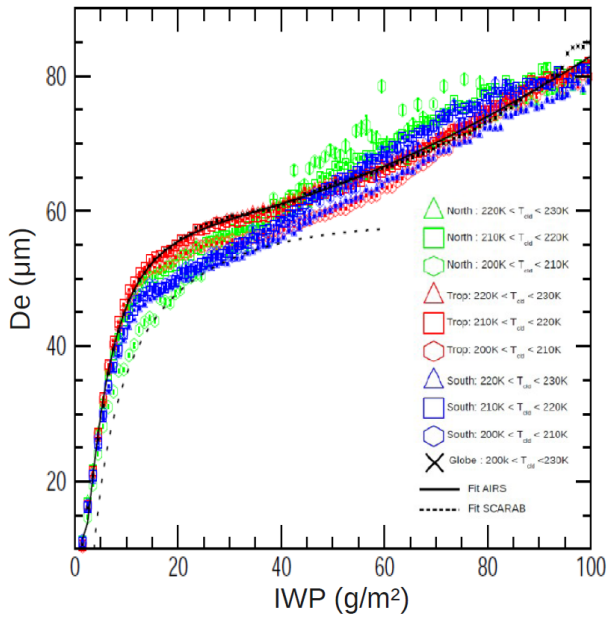

Fig. 15. Relationship between D_e and IWP, as retrieved from AIRS observations for ST-HICs. Results are shown for three latitude bands, separately for three temperature intervals. The global annual dependence is also shown (black cross), as well as the parameterization of Eq. (4) (black line). Statistics is over the period 2003–2009.

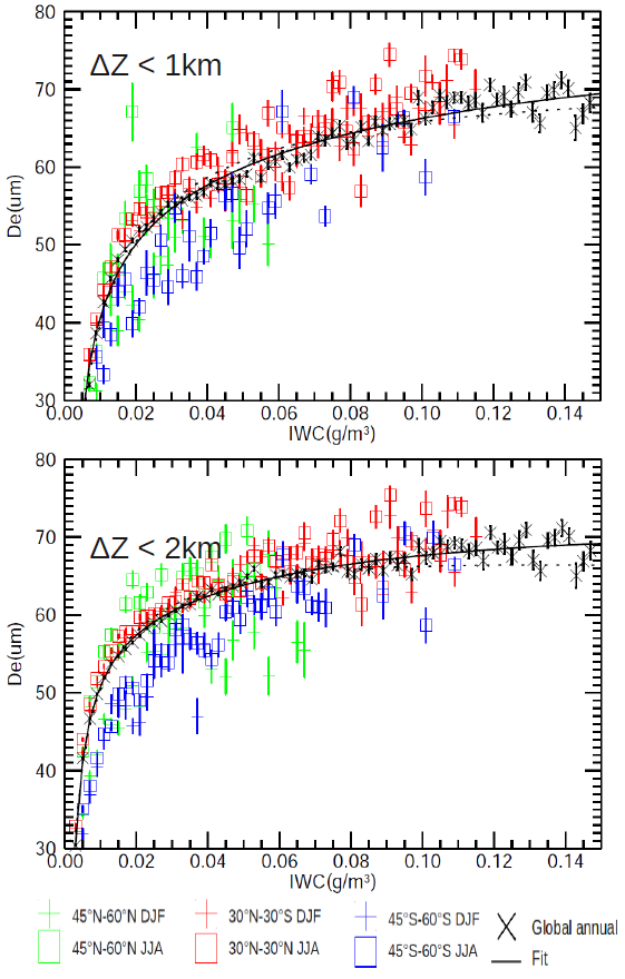

Fig. 16. Relationship between D_e and an estimation of the average IWC for ST-HICs with vertical extent between 0.5 and 1 km (top) and between 0.5 and 2 km (bottom). Results are shown for three latitude bands in boreal summer and in boreal winter. The global annual dependence is also shown (black cross), as well as the parameterization of Eq. (5) (black line). For comparison is shown parameterization developped in McFarquhar et al. (2003) (black dashed lines). Statistics is over the period 2007–2008.

each pressure layer in which there is enough humidity to form clouds. The vertical cloud extent is determined by the number of adjacent cloud layers. However, it should be noted that this kind of parameterization depends for geometrically thicker clouds on the position relative to the cloud top. Therefore, it could be interesting for radiative flux computations to use the parameterization of D_e by IWP.

6 Conclusions

In this article we have presented a retrieval method and a climatological analysis of the bulk microphysical properties of semi-transparent ice clouds using AIRS observations. The retrieval is based on a look-up table approach, for which cirrus emissivities in the spectral range between 8 and 12 µm have been simulated as a function of D_e and IWP. Therefore single scattering properties of randomly oriented column-like or aggregate-like ice crystals, distributed according to a bimodal-Γ size distribution, have been implemented into the radiative transfer model 4A, coupled with the multiple scattering model DISORT, based on discrete ordinate radiative transfer. Sensitivity studies lead in general to similar conclusions as an earlier study using TOVS data by Rädel et al. (2003). Global biases due to assumptions on cloud and atmospheric properties as well as on ice crystal habit are on average less than 5 % with a noise less than 5 %. Mean biases linked to assumptions of horizontal homogeneity are also on average less than 5 % and therefore smaller than for TOVS, essentially because of spatial and spectral resolution improvements of the AIRS instrument. The use of six channels between 8.5 and 12.5 µm allows a distinction between column-like and aggregate-like ice crystals. The retrieval is applicable to high clouds with an effective emissivity from 0.2 to 0.85, increasing the interval 0.3 to 0.85 in the TOVS retrieval. The relationship between retrieved bulk microphysical properties and cloud temperature revealed that super-cooled water droplets may exist and influence the retrieval down to temperatures of 230 K. This is consistent with theoretical and in-situ studies. Therefore, the retrieval of

bulk microphysical properties using AIRS data only considers semi-transparent high ice clouds (ST-HIC) that represent almost 15 % of all clouds and up to 30 % of high clouds during midlatitude winter. About 60 % of all ST-HICs contain aggregate-like ice crystals. Column-like ice crystals are more often found in ST-HICs over land, probably linked to a smaller IWP. For these clouds, D_e and IWP slightly increase with cloud temperature, with a regional and seasonal spread. On average cloud emissivity, IWP and D_e, as well as vertical extent and amount of multiple cloud layers present seasonal cycles in the midlatitudes. Whereas the NH midlatitudes show more seasonal difference in cloud emissivity, IWP and vertical extent, the SH midlatitudes show a larger seasonal difference in D_e, and fraction of aggregate-like ice crystal habit. These differences have to be studied further in relation with dynamical parameters. The use of the Radar-Lidar GEOPROF data demonstrates that the retrieved bulk microphysical properties essentially depends on cloud optical thickness (or emissivity) and are almost independent of their vertical extent. The comparison with TOVS has shown a good agreement on the overall distributions. Nevertheless, the better spatial resolution and deeper sounding of AIRS due to the use of additional channels leads to an increased sensitivity on microphysical properties for optically thin and thicker cirrus. We used this global data set to study relationships between cloud bulk microphysical properties of relevance to GCM parametrizations. Whereas the relationship between D_e and cloud temperature is only weak and depends on many other factors, we have shown that a parameterization of D_e as a function of IWP is more robust. The spread of D_e due to other factors is less than 10 µm. By using the synergy with Radar-Lidar GEOPROF data and assuming a vertically constant IWC, we have also investigated a parameterization of D_e as a function of IWC for cirrus with relatively small vertical extent, in agreement with in situ observations. However, it should be noted that this kind of parameterization depends for geometrically thicker clouds on the position relative to the cloud top. Further investigations are necessary on D_e and IWC profiles on a global scale, using combined retrievals of CALIPSO and CloudSat. In the meantime, it could be interesting for radiative flux computations to use a parameterization between D_e and IWP.

Acknowledgements. This work has been financially supported by CNRS and CNES. The authors thank the members of the AIRS, CALIPSO and CloudSat science teams for their efforts and cooperation in providing the data as well as the engineers and space agencies who control the quality of the data. The authors want to thank two anonymous reviewers for their very fruitful comments that improved the clarity of this manuscript. We also want to thank our former colleagues Sylvain Cros and Nicolas Lamquin for their technical support.

Edited by: T. Garrett

The publication of this article is financed by CNRS-INSU.

References

Ackerman, S. A., Smith, W. L., Collard, A. D., Ma, X. L., Revercomb, H. E., and Knuteson, R. O.: Cirrus cloud properties derived from high-spectral resolution infrared spectrometry during FIRE II, Part II: Aircraft HIS results, J. Atmos. Sci., 52, 4246–4263, 1995.

Arnott, W. P., Dong, Y. Y. and Hallett, J.:Extinction efficiency in the infrared A2 18 mmB of laboratory ice clouds: observations of scattering minima in the Christiansen bands of ice, J. Opt. Soc. Am., 34, 541–551, 1995.

Aumann, H. H., Chahine, M. T., Gautier, C., Goldberg, M. D., Kalnay, E., McMillin, L. M., Revercomb, H., Rosenkranz, P. W., Smith, W. L., Staelin, D. H. Strow, L. L., and Susskind, J.: AIRS/AMSU/HSB on the Aqua mission: Design, science objectives, data products, and processing systems, IEEE T. Geosci. Remote, 41, 253–264, 2003.

Baran, A.: On the scattering and absorption properties of cirrus cloud, J. Quant. Spectrosc. Ra., 89, 17–36, 2004.

Baran, A. J. and Francis, P. N.: On the radiative properties of cirrus cloud at solar and thermal wavelengths: A test of model consistency using high-resolution airborne radiance measurements, Q. J. Roy. Meteor. Soc., 130, 763–778, 2004.

Baran, A. J., Francis, P. N., Havemann, S., and Yang, P: A study of the absorption and extinction properties of hexagonal ice columns and plates in random and preferred orientation, using exact T-matrix theory and aircraft observations of cirrus, J. Quant. Spectrosc. Ra., 70, 505–518, 2001.

Baran, A. J., Connolly, P. J., and Lee, C.: Testing an ensemble model of cirrus ice crystals using midlatitude in situ estimates of ice water content,volume extinction coefficient and the total solar optical depth, J. Quant. Spectrosc. Ra., 110, 1579–1598, 2009.

Boehm, M. T. and Lee, S.: The Implications of Tropical Rossby Waves for Tropical Tropopause Cirrus Formation and for the Equatorial Upwelling of the Brewer-Dobson Circulation, J. Atmos Sci., 60, 247–261, 2003.

Bony, S. and Emanuel, K. A.: A Parameterization of the Cloudiness Associated with Cumulus Convection; Evaluation Using TOGA COARE Data, J. Atmos Sci., 58, 3158–3183, 2001.

Boudala, F. S., Isaac, G. A., Fu, Q., and Cober, S. G.: Parameterization of effective ice particle size for high-latitude clouds, Int. J. Climatol., 22, 1267–1284, 2002.

Chahine, M. T., Pagano, T. S., Aumann, H. H., Atlas, R., Barnet, C., Blaisdell, J., Chen, L., Divakarla, M., Fetzer, E. J., Goldberg, M., Gautier, C., Granger, S., Hannon, S., Irion, F. W., Kakar, R., Kalnay, E., Lambrigtsen, B. H., Lee, S., Marshall, J. L., McMillan, W. W., McMillin, L., Olsen, E. T., Revercomb, H., Rosenkranz, P., Smith, W. L., Staelin, D., Strow, L. L., Susskind, J., Tobin, D., Wolf, W., and Zhou, L.: AIRS: Improving weather

forecasting and providing new data on greenhouse gases, B. Am. Meteor. Soc., 87, 911–926, 2006.

Chédin, A., Scott, N. A., Wahiche, C., and Moulinier, P.: The improved initialization inversion method: A high resolution physical method for temperature retrievals from satellites of the TIROS-N series, J. Appl. Meteor., 24, 128–143, 1985.

Chepfer, H., Bony, S., Winker, D., Cesana, G., Dufresne, J. L., Minnis, P., Stubenrauch, C. J., and Zeng, S.: The GCM-Oriented CALIPSO Cloud Product (CALIPSO-GOCCP), J. Geophys. Res., 115, D00H16, doi:10.1029/2009JD012251, 2010.

Chevallier, F., Cheruy, F., Scott, N. A., and Chédin, A.: A neural network approach for a fast and accurate computation of longwave radiative budget, J. Appl. Meteor., 37, 1385–1397, 1998.

Chung, S. G., Ackerman, S. A., Van Delst, P. F., and Menzel, W. P.: Model Calculations and Interferometer Measurements of Ice-Cloud Charancteristics, J. Appl. Meteor., 39, 634–644, 2000.

Cooper, S. J., L'Ecuyer, T. S., Gabriel, P., Baran, A. J., and Stephens, G. L.: Performance assessment of a five-channel estimation-based ice cloud retrieval scheme for use over the global oceans, J. Geophys. Res., 112, D04207, doi:10.1029/2006JD007122, 2007.

Donner, L. J., Seman, C. J., Soden, B. J., Hemler, R. S., and Warren, J. C.: Large-scale ice clouds in the GFDL SKYHI general circulation model, J. Geophys. Res., 102, 745–768, 1997.

Doutriaux-Boucher, M.: Evaluation of cloud thermmodynamic phase parametriization in the LMDZ GCM by using POLDER staellite data, Geophys. Res. Lett., 31, L06126, doi:10.1029/2003GL019095, 2004.

Edwards, J. M., Havemann, S., Thelen, J.-C., and Baran, A. J.: A new parametrization for the radiative properties of ice crystals: Comparison with existing schemes and impact in a GCM, Atmos. Res., 83, 19–35, 2007.

Field, P. R. and Wood, R.: Precipitation and Cloud Structure in Midlatitude Cyclones, J. Climate, 20, 233–254, doi:10.1175/2007JAS2344.1, 2007.

Field, P. R., Hogan, R. J., Brown, P. R., Illingworth, A. J., Choularton, T. W., and Cotton, R. J.: Parametrization of ice-particle size distributions for mid-latitude stratiform cloud, Q. J. Roy. Meteor Soc., 131, 1997–2017, 2005.

Field, P. R., Heymsfield, A. J., and Bansemer, A.: Shattering and Particle Interarrival Times Measured by Optical Array Probes in Ice Clouds, J. Atmos. Oceanic Technol., 23, 1357–1371, 2006.

Francis, P. N., Foot, J. S., and Baran A. J.: Aircraft measurements of the solar and infrared radiative properties of cirrus and their dependence on ice crystal shape, J. Geophys. Res., 104, 685–695, 1999.

Garrett, T. J., Heymsfield, A. J., McGill, M. J., Ridley, B. A., Baumgardner, D. G., Bui, T. P., and Webster, C. R.: Convective generation of cirrus near the tropopause, J. Geophys. Res., 109, D21203, doi:10.1029/2004JD004952, 2004.

Gayet, J.-F., Mioche, G., Shcherbakov, V., Gourbeyre, C., Busen, R., and Minikin, A.: Optical properties of pristine ice crystals in mid-latitude cirrus clouds: a case study during CIRCLE-2 experiment, Atmos. Chem. Phys., 11, 2537–2544, doi:10.5194/acp-11-2537-2011, 2011.

Giraud, V., Thouron, 0., Riedi, J., and Goloub, P.: Analysis of direct comparison of cloud top temperature and infrared split window signature against independant retrievals of cloud thermodynamic phase, Geophys. Res. Lett., 28, 983–986, 2001

Heymsfield, A. J.: Properties of Tropical and Midlatitude Ice Cloud Particle Ensembles. Part II:Applications for Mesoscale and Climate Models, J. Atmos. Sci., 60, 2592–2611, 2003.

Heymsfield, A. J. and Platt, C. M. R.: A Parameterization of the Particle Size Spectrum of Ice Clouds in Terms of the Ambient Temperature and the Ice Water Content, J. Atmos. Sci., 41, 846–855, 1984.

Heymsfield, A. J., Matrosov, S., and Baum, B.: Ice Water Path-optical Depth ReLationships for Cirrus and Deep stratiform ice cloud layers, J. Appl. Meteorol., 42, 1369–1387, 2002.

Hilton, F., Armante, R., August, T., Barnet, C., Bouchard, A., Camy-Peyret, C., Capelle, V., Clarisse, L., Clerbaux, C., Coheur, P.-F., Collard, A., Crevoisier, C., Dufour, G., Edwards, D., Faijan, F., Fourrié, N., Gambacorta, A., Goldberg, M., Guidard, V., Hurtmans, D., Illingworth, S., Jacquinet-Husson, N., Kerzenmacher, T., Klaes, D., Lavanant, L., Masiello, G., Matricardi, M., McNally, A., Newman, S., Paveli, E., Payan, S., Péquignot, E., Peyridieu, S., Phulpin, T., Remedios, J., Schlssel, P., Serio, C., Strow, L., Stubenrauch, C. J., Taylor, J., Tobin, D., Wolf, W., and Zhou, D.: Hyperspectral Earth Observation from IASI, B. Am. Meteor. Soc., doi:10.1175/BAMS-D-11-00027.1, in press, 2012.

Hong, G., Yang, P., Gao, B.-C., Baum, B. A., Hu, Y. X., King, M. D., and Platnik, S.: High Cloud Properties from Three Years of MODIS Terra and Aqua Collection-4 Data over the Tropics, J. Appl. Meteorol. Clim., 46, 1840–1856, 2007.

Hu, Y. and Winker, D.: Caliop Cloud Phase Discrimination Algorithm, J. Atmos. Oceanic Technol., 26, 2293–2309, doi:10.1175/2009JTECHA1280.1, 2009.

Ivanova, D., Mitchell, D. L., Arnotta, W. P., and Poellotb, M.: A GCM parameterization for bimodal size spectra and ice mass removal rates in mid-latitude cirrus clouds, Atmos. Res., 59–60, 89–113, 2001.

Kahn, B. H., Eldering, A., Ghil, M., Bordoni, S., and Clough, S. A.: Sensitivity Analysis of Cirrus Cloud Properties from High-Resolution Infrared Spectra. Part I: Methodology and Synthetic Cirrus, J. Climate, 17, 4856–4870, 2004.

Kahn, B. H., Eldering, A., Braverman, A. J., Fetzer, E. J., Jiang, J. H., Fishbein, E., and Wu, D. L.: Toward the characterization of upper tropospheric clouds using Atmospheric Infrared Sounder and Microwave Limb Sounder observations, J. Geophys. Res., 112, D05202, doi:10.1029/2006JD007336, 2007.

Kahn, B. H., Liang, C. K., Eldering, A., Gettelman, A., Yue, Q., and Liou, K. N.: Tropical thin cirrus and relative humidity observed by the Atmospheric Infrared Sounder, Atmos. Chem. Phys., 8, 1501–1518, doi:10.5194/acp-8-1501-2008, 2008.

Kristjánsson, J. E., Edwards, J. M., and Mitchell, D. L.: Impact of a new scheme for optical properties of ice crystals on climates of two GCMs, J. Geophys. Res., 105, 10063–10079, 2000.

Korolev, A. and Isaac, G.: Roundness and aspects ratios of particles in ice clouds, J. Atmos., 60, 1795–1808, 2003.

Korolev, A. V. and Isaac, G. A.: Shattering during Sampling by OAPs and HVPS. Part I: Snow Particles, J. Atmos. Ocean Tech., 22, 528–542, 2004.

Korolev, A. V., Isaac, G. A., Mazin, I. P., and Barker, H. W.: Microphysical properties of continental clouds from in-situ measurements, Q. J. Roy. Meteor. Soc., 127, 2117–2151, 2001.

L'Ecuyer, T. S., Gabriel, P., Leesman, K., Cooper, S. J., and Stephens, G. L.: Objective assessment of the information content of visible and infrared radiance measurements for cloud micro-

physical property retrievals over the global oceans. Part I: Liquid clouds, J. Appl. Meteor. Climatol., 45, 20–41, 2006.

Liou, K. N., Gu, Y., Yue, Q., and McFarguhar, G.: On the correlation between ice water content and ice crystal size and its application to radiative transfer and general circulation models, Geophys. Res. Lett, 35, L13805, doi:10.1029/2008GL033918, 2008.

Luo, Z. and Rossow, W. B.: Characterizing Tropical Cirrus Life Cycle, Evolution, and Interaction with Upper-Tropospheric Water Vapor Using Lagrangian, J. Climate, 17, 4541–4563, 2004.

Lynch, D. K., K. Sassen, D. O.-C. Starr, and Stevens, G.: Cirrus, 480 pp., Oxford Univ. Press, New York, 480 pp., 2002.

Mace, G. G., Sassen, K., Kinne, S., and Ackerman, T. P.: An examinationo f cirrus cloud characteristicsu singd ata from millimeter wave radar and lidar: The 24 April SUCCESS casestudy, Geophys. Res. Lett., 25, 1133–1136, 1998.

Mace, G. G., Zhang, Q., Vaughan, M., Marchand, R., Stephens, G., Trepte, C., and Winker, D.: A description of hydrometeor layer occurrence statistics derived from the first year of merged Cloudsat and CALIPSO data, J. Geophys. Res., 114, D00A26, doi:10.1029/2007JD009755, 2009.

Martins, E., Noel, V., and Chepfer, H.: Properties of cirrus and subvisible cirrus from nighttime Cloud-Aerosol Lidar with Orthogonal Polarization (CALIOP), related to atmospheric dynamics and water vapor, J. Geophys. Res., 116, D02208, doi:10.1029/2010JD014519, 2011.

McFarlane, N. A., Boer, G. J., Blanchet, J.-P., and Lazare, M.: The canadian climate Centre second-generation general circulation model and its equilibrium climate, J. Climate, 5, 1013–1044, 1992.

McFarquhar, G. and Heymsfield, A. J.: Microphysical characteristics of three anvils sampled during the Central Equatorial Pacific experiment, J. Atmos. Sci, 53, 2401–2423, 1996.

McFarquhar, G. and Heymsfield, A. J.: Parameterization of Tropical Cirrus Ice Crystal Size Distributions and Implications for Radiative Transfer: Results from CEPEX, J. Atmos. Sci., 54, 2187–2200, 1997a.

McFarquhar, G. and Heymsfield, A. J.: The Definition and Significance of an Effective Radius for Ice Clouds, J. Atmos. Sci., 55, 2039–2052, 1997b.

McFarquhar, G., Iacobellis, S., and Somerville, C. J.: SCM Simulations of Tropical Ice Clouds Using Observationally Based Parameterizations of Microphysics, J. Climate, 16, 1643–1664, 2003.

McFarquhar, G., Um, J., Freer, M., Baumgardner, D., Kok, G. L., and Mace, G.: Importance of small ice crystals to cirrus properties: Observations from the Tropical Warm Pool International Cloud Experiment (TWP-ICE), Geophys. Res. Lett., 34, L13803, doi:10.1029/2007GL029865, 2007.

Mitchell, D.: Effective Diameter in Radiation Transfer: General Definition, Applications and Limitations, J. Atmos. Sci., 59, 2330–2346, 2002.

Mitchell, D. L.: Inferring cirrus size distributions through satellite remote sensing and microphysical databases, J. Atmos. Sci., 67, 1106–1125, 2009.

Mitchell, D. L., Chai, S. K., and Liu, Y.: Modeling cirrus clouds, I. Treatment of bimodal size spectra and case study analysis, J. Atmos. Sci., 53, 2952–2966, 1996a.

Mitchell, D. L., Macke, A., and Liu, Y.: Modeling cirrus clouds, II, Treatment of radiative properties, J. Atmos. Sci., 53, 2967–2988, 1996b.

Mitchell, D. L., Baran, A. J., Arnott, W. P., and Schmitt, C.: Testing and comparing the modified anomalous diffraction approximation, J. Atmos. Sci., 63, 2948–2962, 2006.

Mitchell, D. L., Lawson, R. P., and Baker, B.: Understanding effective diameter and its application to terrestrial radiation in ice clouds, Atmos. Chem. Phys., 11, 3417–3429, doi:10.5194/acp-11-3417-2011, 2011.

Ou, S. C., Liou, K. N., Takano, Y., Rao, N. X., Fu, Q., Heymsfield, A. J., Miloshevich, L. M., Baum, B., and Kinne, S. A.: Remote sounding of cirrus cloud optical depths and ice crystal sizes from AVHRR data: Verification using FIRE II IFO measurements, J. Atmos. Sci., 52, 4143–4158, 1995.

Pavolonis, M. J.: Advances in Extracting Cloud Composition Information from Spaceborne Infrared Radiances-A Robust Alternative to Brightness Temperatures. Part I: Theory, J. Appl. Meteor. Climatol., 49, 1992–2012, 2010.

Péquignot, E., Céhdin, A., and Scott, N. A.: Infrared continental surface emissivity spectra retrieved from AIRS hyperspectral sensor, J. Appl. Meteor. Climatol., 47, 1619–1633, 2008.

Platnick, S., King, M. D., Ackerman, S. A., Menzel, W. P., Baum, B. A., Riédi, J. C., and Frey, R. A.: The MODIS Cloud Products: Algorithms and Examples From Terra, IEEE T. Geosci. Remote., 41, 459–473, 2003.

Pierangelo, C., Mishchenko, M., Balkanski, Y., and Céhdin, A.: Retrieving the effective radius of Saharan dust coarse mode from AIRS, Geophys. Res. Lett., 32, L20813, doi:10.1029/2005GL023425, 2005.

Rädel, G., Stubenrauch, C. J., and Holtz, R.: Retrieval of effective ice crystal size in the infrared: Sensitivity study and global measurments from TIROS-N Operationnal Vertical Sounder, J. Geophys. Res., 108, 4281, doi:10.1029/2002JD002801, 2003.

Riedi, J., Marchant, B., Platnick, S., Baum, B. A., Thieuleux, F., Oudard, C., Parol, F., Nicolas, J.-M., and Dubuisson, P.: Cloud thermodynamic phase inferred from merged POLDER and MODIS data, Atmos. Chem. Phys., 10, 11851–11865, doi:10.5194/acp-10-11851-2010, 2010.

Roebeling, R. A., Feijt, A. J., and Stammes, P.: Cloud property retrievals for climate monitoring: Implications of differences between Spinning Enhanced Visible and Infrared Imager (SEVIRI) on METEOSAT-8 and Advanced Very High Resolution Radiometer (AVHRR) on NOAA-17, J. Geophys. Res., 111, D20210, doi:10.1029/2005JD006990, 2006.

Rossow, W. B. and Schiffer, R. A.: Advances in understanding clouds from ISCCP, B. Am. Meteor. Soc., 80, 2261–2287, 1999.

Sassen, K. and Dodd, G. C.: Homogeneous nucleation rate for highly supercooled cirrus cloud droplets, J. Atmos. Sc., 45, 1357–1369, 1988.

Scott, N. A., and Chédin A.: A fast line-by-line method for atmospheric absorption computations: the 4A Automized Atmospheric Absorption Atlas, J. Appl. Meteor., 20, 801–812, 1981.

Seemann, S. W., Borbas, E. E., Knuteson, R. O., Stephenson, G. R., and Huang, H. L.: Development of a Global Infrared Land Surface Emissivity Database for Application to Clear Sky Sounding Retrievals from Multispectral Satellite Radiance Measurements, J. Appl. Meteor. Climatol., 47, 108–123, doi:10.1175/2007JAMC1590.1, 2008.

Seo, E. K. and Liu, G.:Determination of 3D Cloud Ice Water Con-

tents by Combining Multiple Data Sources rom Satellite, Ground Radar, and a Numerical Model, J. Appl. Metorol., 45, 1494–1504, 2006.

Smith, W. L., Woolf, H. M., Hayden, M. C., Wark, D. Q., and McMillin, L. M.: The TIROS-N Operational Vertical Sounder, B. Am. Meteorol. Soc., 60, 1177–1187, 1979.

Stamnes, K., Tsay, S., Wiscombe, W., and Jayaweera, K.: Numerically stable algorithm for discrete-ordinate-method radiative transfer in multiple scattering and emitting layered media, Appl. Optics, 27, 2502–2509, 1988.

Stith, J. L., Dye, A. E., Bansemer, A., and Heymsfield, J. A.: Microphysical Observations of Tropical Clouds, J. Appl. Metorol., 41, 97–117, 2002.

Stephens, G. L., Vane, D. G., Boain, R. J., Mace, G. G., Sassen, K., Wang, Z., Illingworth, A. J., O'Connor, E. J., Rossow, W. B., Durden, S. L., Miller, S. D., Austin, R. T., Benedetti, A., and Mitrescu, C.: The CloudSat mission and the A-train, B. Am. Meteor. Soc., 83, 1771–1790, 2002.

Stubenrauch, C. J., Holz, R., Chédin, A., Mitchell, D. L., and Baran, A. J: Retrieval of cirrus ice crystal sizes from 8.3 and 11.1 μm emissivities determined by the improved initialization inversion of TIROS-N Operational Vertical Sounder observations, J. Geophys. Res., 104, 793–808, 1999.

Stubenrauch, C. J., Eddounia, F., and Rädel, G.: Correlations between microphysical properties of large-scale semi-transparent cirrus and the state of the atmosphere, Atmos. Res., 72, 403–423, 2004.

Stubenrauch, C. J., Chédin, A., Rädel, G., Scott, N. A., and Serra, S.: Cloud Properties and Their Seasonal and Diurnal Variability from TOVS Path-B, J. Climate, 19, 5531–5553 2006.

Stubenrauch, C. J., Eddouina, F., Edwards, J. M., and Macke, A.: Evaluation of Cirrus Parameterizations for Radiative Flux Computations in Climate Models Using TOVSScaRaB Satellite Observations, J. Climate, 20, 4459–4475, doi:10.1175/JCLI4251.1, 2007.

Stubenrauch, C. J., Cros, S., Lamquin, N., Armante, R., Chédin, A., Crevoisier, C., and Scott, N. A.: Cloud properties from AIRS and evaluation with CALIPSO, J. Geophys. Res., 113, D00A10, doi:10.1029/2008JD009928, 2008.

Stubenrauch, C. J., Cros, S., Guignard, A., and Lamquin, N.: A 6-year global cloud climatology from the Atmospheric InfraRed Sounder AIRS and a statistical analysis in synergy with CALIPSO and CloudSat, Atmos. Chem. Phys., 10, 7197–7214, doi:10.5194/acp-10-7197-2010, 2010.

Susskind, J., Barnet C., and Blaisdell J.: Retrieval of atmospheric and surface parameters from AIRS/AMSU/HSB data in the presence of clouds, IEEE T. Geosci. Remote, 41, 390–409, 2003.

Susskind, J., Barnet, C., Blaisdell, J., Iredell, L., Keita, F., Kouvaris, L., Molnar, G., and Chahine, M.: Accuracy of geophysical parameters derived from AIRS/AMSU as a function of fractional cloud cover, J. Geophys. Res., 111, D09S17, doi:10.1029/2005JD006272, 2006.

Tobin, D. C., Revercomb, H. E., Knuteson, R. O., Lesht, B. M., Strow, L. L., Hannon, S. E., Feltz, W. F., Moy, L. A., Fetzer, E. J., and Cress, T. S.: Atmospheric Radiation Measurement site atmospheric state best estimates for Atmmospheric Infrared Sounder temperature and water vapour retrieval validation, J. Geophys. Res., 111, D09S14, doi:10.1029/2005JD006103, 2006.

Wang, J., Rossow, W. B., and Zhang, Y.: Cloud Vertical Structure and its Variations from a 20-Yr Global Rawinsonde Dataset, J. Climate, 13, 3041–3056, 2000.

Winker, D. M., Pelon, J. R., and McCormick, M. P.: The CALIPSO mission: Spaceborne lidar for observation of aerosols and clouds, Proceedings of SPIE, 4893, 1–11, 2003.

Winker, D. M., Hunt, W. H., and McGill, M. J.:Initial performance assessment of CALIOP, Geophys. Res. Lett., 34, L19803, doi:10.1029/2007GL030135, 2007.

Winker, D., Getzewitch, B., and Vaughan, M.: Evaluation and Applications of Cloud Climatologies from CALIOP, Proc. Int. Laser Radar Conference (ILRC), 2008.

Winker, D. M., Vaughan, M. A., Omar, A., Hu, Y., and Powell, K. A.: Overview of the CALIPSO mission and CALIOP data processing algorithms, J. Atmos. Ocean. Tech., 26, 2310–2323, 2009.

Wylie, D. and Menzel, W. P: Four Years of Global Cirrus Cloud Statistics Using HIRS, J. Climate, 7, 1972–1986, 1994.

Wylie, D. and Menzel, W. P: Eight Years of High Cloud Statistics Using HIRS, J. Climate, 12, 170–184, 1999.

Wylie, D., Jackson, D. L., Menzel, W. P., and Bates, J. J.: Trends in Global Cloud Cover in Two Decades of HIRS Observations, J. Climate, 18, 3021–3031, 2005.

Wyser, K. and Yang, P.: Average ice crystal size and bulk shortwave single-scattering properties of cirrus clouds, Atmos. Res., 49, 315–335, 1998.

Yang, P., Weia, H.-L., and Baumb, B. A.: The spectral signature of mixed-phase clouds composed of non-spherical ice crystals and spherical liquid droplets in the terrestrial window region, J. Quant. Spectrosc. Ra., 79–80, 1171–1188, 2002.

Yue, Q. and Liou, K. N.: Cirrus cloud optical and microphysical properties determined from AIRS infrared spectra, Geophys. Res. Lett., 36, L05810, doi:10.1029/2008GL036502, 2009.

Yue, Q., Liou, K. N., Ou, S. C., Kahn, B. H., Yang, P., and Mace, G.: Interpretation of AIRS data in thin cirrus atmospheres based on a fast radiative transfer model, J. Atmos. Sci., 64, 3827–3842, 2007.